

ABSTRACT

WU, XIAOTIAN. Surface Modification of Polylactic Acid Nonwoven Webs. (Under the direction of Dr. Martin W. King.)

The goal of this research was to use a number of surface modification technologies to improve the surface properties of tissue engineering scaffolds that would be biocompatible and support the growth and proliferation of cells. Polylactic acid (PLA) nonwoven fabric, obtained from Ahlstrom Nonwovens LLC, was used as the scaffold material. Three different surface modification methods: UV, UV/Ozone, and plasma were studied with the objective of polymerizing acrylamide monomer onto the surface of PLA nonwoven fabric.

Acrylamide was used as the monomer since it contains amino groups which can readily react with other functional groups. The plasma initiated grafting led to a fall in contact angle of 32 degrees while UVO grafting caused the contact angle to fall to 56 degrees whereas UV led to a contact angle of 113 degrees. This suggests that plasma initiation is a more effective way of grafting acrylamide onto a PLA surface without influencing the bulk properties.

After surface functionalization, genipin was attached to the surface of the PLA nonwoven webs, serving as a spacer molecule between the amino groups in acrylamide and the amine groups in collagen. This is because collagen was immobilized onto the genipin treated PLA surface for better biocompatibility. It is believed that the genipin spacer molecule was able to reduce steric problems between the functional groups on the PLA and protein molecules.

TOF-SIMS analysis demonstrated a bioactive collagen coating had been successfully immobilized. However, the uniformity of this coating could be improved.

Surface Modification of Polylactic Acid Nonwoven Webs

by
Xiaotian Wu

A thesis submitted to the Graduate Faculty of
North Carolina State University
in partial fulfillment of the
requirements for the degree of
Master of Science

Textile Engineering

Raleigh, North Carolina

2012

APPROVED BY:

Martin W. King
Chair of Advisory Committee

Ahmed El-Shafei
Co-chair of Advisory Committee

Julie Willoughby
Member of Advisory Committee

© Copyright 2012 by Xiaotian Wu

All Rights Reserved

DEDICATION

To my beloved family!

BIOGRAPHY

Xiaotian Wu was born on March 5th, 1989 in China. She attended Tongxiang High School for 3 years and got admission from Donghua University in September, 2007. In June 2011, she received her Bachelor of Science degree in Textile Engineering. In pursuit of graduate studies, Xiaotian was accepted into the College of Textiles of North Carolina State University in the Fall 2010 and she was appointed as a research assistant in Fall 2011. During the two years in the College of Textiles, she was able to join Dr. Martin King's biomedical textiles research group. After completion of this program and receiving her Master's degree, she plans to continue expanding her study in Biostatistics and Bioinformatics at Duke University.

ACKNOWLEDGMENTS

First of all, I would like to express my sincere gratitude towards the College of Textiles, North Carolina State University for offering me a great opportunity to further my education in the field of textiles. During two years, I have gained first hand skills in proposal writing, reviewing the literature and experimental laboratory techniques.

I would also like to thank my advisor, Dr. Martin King who played an important role in my academic life. He is experienced in the area of biomedical materials and has always been ready to help me. His knowledge and support throughout my two years in the College of Textiles are greatly appreciated. I am always inspired by his humor, kindness and erudition. His encouragement will accompany me throughout my entire life.

Meanwhile, I also appreciate the support given by the other members of my Advisory Committee, Dr. Ahmed El-Shafei and Dr. Julie Willoughby. The discussions with them have been most helpful in completing this project. They have offered precious and effective suggestions about my research approach and have generously provided their equipment for me to use. This research would not have been possible without their kind support.

Moreover, many other people have helped me during these two years. I would like to thank Birgit Anderson, Jeff Krauss, Chuck Mooney, Fred Stevie, Judy Elson, Vidya Viswanath, Ting He, Nisarg Tambe, Lu Liu, Rashi Grewal and Amsarani Ramamoorthy for advising me about the use of various items of lab equipment and providing their expertise. I should also thank Dr. Liu Song who is a professor in University of Manitoba, Canada. He has already undertaken relevant surface modifications to PET fabrics and gave me suggestions for my project.

Last but not the least, I would like to express my deep love and gratitude to my dear parents and grandparents in China who have always supported me throughout my life. Without their personal encouragement I could not have achieved so much or be where I am right now. I am also very grateful to all my friends here in North Carolina State University since they always give me a helping hand when I am down. I could not have survived from such a severe challenge of completing this master's degree without their help.

TABLE OF CONTENTS

LIST OF TABLES.....	xi
LIST OF FIGURES.....	xii
CHAPTER 1- INTRODUCTION.....	1
1.1. Background.....	1
1.2. Goals and objectives.....	2
1.3. Limitations.....	4
CHAPTER 2-REVIEW OF LITERATURE.....	5
2.1. TISSUE ENGINEERING.....	5
2.1.1. Background.....	5
2.1.2. Definition.....	6
2.2. SCAFFOLDS.....	8
2.2.1. Overview.....	8
2.2.2. Materials.....	9
2.2.2.1. Natural scaffolds.....	10
2.2.2.2. Synthetic scaffolds.....	11
2.2.2.3. Multi-material scaffolds.....	13
2.3. SURFACE MODIFICATION.....	14
2.3.1. Overview.....	14
2.3.2. Concept of surface modification.....	15
2.3.3. Techniques in surface modification.....	16
2.3.3.1. UV irradiation.....	16

2.3.3.2. UV/O ₃ irradiation.....	17
2.3.3.3. Plasma treatment.....	17
2.4. IMMOBILIZATION OF BIOACTIVE COMPOUNDS.....	19
2.5. SURFACE CHARACTERIZATION METHODS.....	21
2.5.1. Fourier transform infrared spectroscopy (FTIR)	22
2.5.2. Water contact angle analysis.....	24
2.5.3. Scanning electron microscopy (SEM)	26
2.5.4. X-ray photoelectron spectroscopy (XPS)	29
2.5.5. Time-of-flight secondary ion mass spectrometry (TOF-SIMS).....	30
CHAPTER 3-EXPERIMENTAL.....	32
3.1. APPROACH OF THIS RESEARCH.....	32
3.2. MATERIALS.....	32
3.2.1. PLA fabric.....	32
3.2.2. Acrylamide.....	34
3.2.3. Potassium persulfate.....	35
3.2.4. Benzophenone.....	35
3.2.5. Genipin	35
3.2.6. Collagen.....	36
3.3. EXPERIMENTAL METHODS.....	36
3.3.1. Surface modification.....	36
3.3.1.1. UV/ozone (UVO) polymerization.....	37
3.3.1.2. Plasma polymerization.....	40

3.3.1.3. UV polymerization.....	43
3.3.2. Genipin attachment.....	44
3.3.3. Collagen immobilization.....	44
3.4. ANALYSIS.....	45
3.4.1. Fabric thickness measurement.....	45
3.4.2. Surface analysis.....	45
3.4.2.1. Contact angle measurements.....	46
3.4.2.2. Fourier transform infrared (FTIR) Spectroscopy.....	47
3.4.2.3. X-ray photoelectron spectroscopy (XPS)	48
3.4.2.4. Time-of-flight secondary ion mass spectrometry (TOF-SIMS).....	50
3.4.3. Surface topography.....	50
3.4.3.1. Scanning electron microscopy (SEM).....	50
3.4.4. Mechanical properties	52
3.4.4.1. Probe bursting strength.....	52
CHAPTER 4-RESULTS AND DISCUSSIONS.....	54
4.1. FABRIC THICKNESS MEASUREMENT.....	54
4.1.1 UVO irradiation.....	54
4.1.2 Plasma treatment.....	55
4.1.3 UV irradiation.....	56
4.2. SURFACE FUNCTIONALIZATION.....	57
4.2.1. UVO polymerization	58
4.2.1.1. Experimental variables.....	60

4.2.1.1.1. Experimental sequence variable.....	60
4.2.1.1.2. Irradiation time variable.....	61
4.2.1.1.3. Monomer concentration variable.....	62
4.2.2. Plasma polymerization	63
4.2.2.1. Experimental variables.....	65
4.2.2.1.1 Plasma intensity.....	65
4.2.2.1.2 Irradiation time.....	66
4.2.2.1.3 Gas type.....	67
4.2.2.1.4 Monomer concentration.....	68
4.2.3. UV polymerization	69
4.3. GENIPIN ATTACHMENT AND COLLAGEN IMMOBILIZATION.....	70
4.3.1. Fourier transform infrared (FTIR) Spectroscopy.....	70
4.3.2. Contact angle.....	72
4.3.3. X-ray photoelectron spectroscopy (XPS)	73
4.3.4. Time-of-flight mass spectrometry (TOF-SIMS)	76
4.4. SURFACE MORPHOLOGY AND FIBER DIAMETER.....	80
4.5. MECHANICAL PROPERTIES.....	85
CHAPTER 5-CONCLUSIONS AND RECOMMENDATIONS	90
5.1. CONCLUSIONS.....	90
5.2. RECOMMENDATIONS.....	91
REFERENCES.....	93
APPENDIX.....	98

A. Contact angle measurements.....	99
B. Fiber diameter measurements.....	102
C. Probe bursting measurements.....	103

LIST OF TABLES

Table 2.1. Cardiac procedures performed in the United States annually.....	5
Table 2.2 Properties of several synthetic polymers used for scaffolds.....	12
Table 2.3. General methods for surface modification.....	14
Table 2.4. Common infrared absorption frequencies.....	23
Table 2.5. Typical contact angle values.....	26
Table 3.1. Thermal properties of the PLA as provided by Ahlstrom Nonwovens LLC.....	33
Table 4.1 Elemental composition of PLA before and after each treatment.....	74

LIST OF FIGURES

Figure 2.1. Basic approach to tissue engineering.....	7
Figure 2.2. 3D image of a porous scaffold.....	8
Figure 2.3. Structure of collagen (a) Model of collagen peptide; (b) Schematic of the triple helix.....	10
Figure 2.4. Elastin structure.....	11
Figure 2.5. Concept of surface modification to improve biological properties.....	15
Figure 2.6. Photografting polymerization initiated by benzophenone.....	16
Figure 2.7. Schematic diagram of the atmospheric-pressure plasma jet.....	18
Figure 2.8. Plasma parameters.....	19
Figure 2.9. Schematic diagram of collagen fibril structure.....	20
Figure 2.10. Principle of ATR system.....	24
Figure 2.11. Contact angle of a liquid droplet onto a solid surface.....	25
Figure 2.12. Schematic view of SEM.....	27
Figure 2.13. Inelastic interaction between primary electrons and electrons in atomic shells.....	28
Figure 2.14. Components of a typical XPS system.....	30
Figure 2.15. Schematic diagram of the SIMS process.....	31
Figure 3.1. Chemical structure of PLA.....	32
Figure 3.2. (a) Optical image of scoured nonwoven PLA fabric..... (b) SEM image of scoured nonwoven PLA fabric.....	34
Figure 3.3. Chemical structure of acrylamide.....	34
Figure 3.4. Chemical structure of benzophenone.....	35

Figure 3.5. Chemical structure of genipin.....	36
Figure 3.6. UVO source. (a) UVOCS system; (b) PLA samples to be irradiated.....	38
Figure 3.7. Atmospheric pressure plasma jet (APPR)	41
Figure 3.8. UV source.....	43
Figure 3.9. OCA 20 DataPhysics optical contact angle measuring system.....	46
Figure 3.10. FTIR equipment.....	47
Figure 3.11. XPS system (Image courtesy of Analytical Instrumentation Facility, NCSU)...	49
Figure 3.12. (a) Sputter coater; (b) SEM equipment.....	51
Figure 3.13. (a) Instron Model 5544 universal mechanical tester.....	53
(b) Compression cage used for probe bursting strength.....	53
Figure 4.1. Thickness of UVO irradiated PLA samples.....	54
Figure 4.2. Thickness of PLA fabric after plasma treatment with different plasma parameters.....	55
Figure 4.3. Thickness of PLA fabric after plasma treatment with different monomer concentrations.....	56
Figure 4.4. Thickness of PLA fabric after UV irradiation.....	56
Figure 4.5. FTIR spectra of the original control PLA sample (in blue) and the PLA sample after exposure to UVO for 10min (in red).....	58
Figure 4.6. FTIR spectra of the original control PLA (in red) and the PLA sample after immersion in acrylamide but without UVO (in blue).....	59
Figure 4.7. Effect of experimental sequence on contact angle.....	60
Figure 4.8. Effect of irradiation time on contact angle.....	61

Figure 4.9. Effect of monomer concentration on contact angle.....	62
Figure 4.10. Surface-droplet interaction during contact angle measurement (a). Control PLA; (b). polyacrylamide grafted PLA.....	63
Figure 4.11. FTIR spectra of original PLA control (in blue) and PLA after 5 minutes of 800W helium plasma treatment (in red).....	64
Figure 4.12. Effect of plasma intensity on contact angle.....	65
Figure 4.13. Effect of irradiation time on contact angle.....	66
Figure 4.14. Effect of gas type on contact angle.....	67
Figure 4.15. Effect of monomer concentration on contact angle.....	68
Figure 4.16. FTIR spectra of original PLA control (in blue) and PLA after 5 minuate of UV irradiation (in red).....	69
Figure 4.17. Effect of UV irradiation time on contact angle.....	70
Figure 4.18. FTIR spectra of PLA under four different surface modification conditions.....	72
Figure 4.19. Contact angle after four different surface modification treatments.....	72
Figure 4.20. Full spectrum of control PLA.....	74
Figure 4.21. Deconvoluted C1s spectrum of control PLA.....	75
Figure 4.22. Full spectrum of acrylamide attached to PLA	75
Figure 4.23. Deconvoluted N1s spectrum of acrylamide attached to PLA.....	76
Figure 4.24. Positive spectra of four PLA samples.....	77
Figure 4.25. Negative spectra of four PLA samples.....	77
Figure 4.26. Chemical mapping images showing overlay of the collagen positive ion image in green over the PLA $C_3H_3O^+$ ion image in red.....	79

Figure 4.27. SEM image of the original PLA control at 1000X (a) and 5000X (b).....80

Figure 4.28. SEM image of PLA after 1min of UVO irradiation at 1000X (a) and 5000X
(b)81

Figure 4.29. SEM image of PLA after 1min of plasma exposure at 1000X (a) and 5000X
(b).....81

Figure 4.30. SEM image of PLA after 5min of UVO irradiation (a), plasma exposure (b) and
UV irradiation (c) at 5000X.....82

Figure 4.31. SEM image of PLA after 15min of UVO irradiation at 1000X(a) and 5000X
(b).....83

Figure 4.32. SEM image of PLA after genipin attachment (a) and collagen immobilization
(b) at 5000X.....83

Figure 4.33. Diameter of PLA fibers before and after treatments.....84

Figure 4.34. Bursting strength of PLA fabric after UVO irradiation.....85

Figure 4.35. Bursting strength of PLA fabric after plasma irradiation.....86

Figure 4.36. Bursting strength of PLA fabric after UV irradiation.....87

Figure 4.37. Comparison of bursting strength of PLA fabric after three different
treatment.....88

Figure 4.38. Bursting strength of PLA fabric before and after treatments.....88

CHAPTER 1-INTRODUCTION

1.1 Background

Over the last decade there has been a growing number of patients with diseased and/or injured organs, who are looking for an organ transplant. However, organ transplantation is currently not the best therapy for many patients because; first, the number of patients needing transplanted organs far exceeds the number of available organs. Second, due to the body's immune response the strong possibility of rejection demands that patients are required to live on a strict regimen of immunosuppressant drugs. This factor should not be neglected ^[1]. Thus, researchers in the medical, clinical and related areas are showing growing interest in the field of tissue engineering and regenerative medicine and devoting themselves to developing viable living tissue substitutes to replace injured tissues and diseased organs.

A tissue engineering scaffold is the basic supportive structure, where cells can be stimulated and cultured in an in vitro bioreactor to promote attachment, proliferation and differentiation into the desired cell phenotype, and hence generate the appropriate type of tissue for implantation back into the patient. Clearly the selection of the material and structure for such a scaffold has certain limitations. For example, the scaffolds should have certain mechanical properties, total porosity, pore size distribution, rate of bioresorption and biocompatibility.

From among the many bioresorbable synthetic polymers, polylactic acid (PLA) has been widely used in orthopedic and other biomedical applications. This is because ^[2]:

1. It is derived from renewable resources such as corn and rice. It slowly degrades and is compostable when put into landfill as garbage. This is environmentally friendly.

2. Once implanted in the body, PLA takes between 9 – 12 months to completely degrade and resorb. This makes it suitable for making into plates and screws for the repair of bone fractures and breaks, which can take 6-9 months to heal.
3. PLA has been shown to have excellent biocompatibility;
4. PLA has good thermal processability compared to other thermoplastic polymers, which makes it easy to manufacture into a range of different products ^[3].

However, limitations still exist for the PLA polymer. For example, initially it has a hydrophobic surface, which makes it difficult for cells to attach, grow and migrate. And because there are few reactive groups present in the polymer structure, it is difficult to attach more reactive groups by surface modification. Various technologies, such as coating, copolymerization, blending of polymers, radio frequency plasma, aerosol spraying, laminating and photografting initiated by UV light and/or ozone, have been developed to modify the surface properties of the PLA polymer for improved physical, chemical and biological performance. In line with these initiatives, the present research study has demonstrated and compared several of these different surface modification techniques.

1.2. Goals and objectives

The overall goal of this study was to determine from among several alternative strategies which technique was the most effective way to modify the surface of a PLA textile material so as to make it biocompatible to the human body. Three different approaches of initiating surface modification using UV light, UV/Ozone irradiation and plasma treatment were

studied to achieve the optimal results. After surface modification, a spacer molecule was attached to link the substrate and the bioactive compound collagen. Then collagen was immobilized onto the genipin treated surface for improved biocompatibility. A series of in vitro tests were carried out to evaluate the properties of the textile material before and after surface treatment and to see if the modified surface could mimic the in vivo environment. Generally speaking, the surface modification was carried out in three steps: 1. Treating the PLA nonwoven surface with various chemical approaches; 2. Attaching a spacer molecule to the functionalized PLA surface; 3. Introducing a bioactive compound, such as collagen, to the treated PLA surface.

The six specific objectives of the study are listed as follows:

- 1) Compare the relative effectiveness of different surface modification techniques to graft a bioactive monomer, e.g. acrylamide, to the surface of PLA fiber using UV light, UV/Ozone irradiation and plasma treatment;
- 2) At each step in the experiment to vary the conditions and determine the most effective combination of process variables to use.
 - a. UV/Ozone irradiation: sequence of experimental steps, irradiation time and monomer concentration;
 - b. Plasma: treatment time, gas intensity, gas type and monomer concentration;
 - c. UV light: irradiation time.

- 3) Compare the mechanical properties of the PLA material after different surface treatments using a probe bursting strength test;
- 4) Identify a spacer molecule and have it attached to the functionalized polymer surface;
- 5) Graft a bioactive coating, e.g. collagen, to the spacer molecule attached PLA surface;
- 6) Evaluate the surface properties of the PLA material before and after surface modification using FTIR, SEM, XPS, contact angle measurements, TOF-SIMS analysis.

1.3. Limitations

The type of PLA nonwoven fabric used in this study is believed to have been fabricated from a poly (L-lactic acid) resin with less than 2% D-isomer. The results of this study, therefore, may not be generalized to apply to other types of PLA resins, e.g. 100% Poly (D-lactic acid) and 100% poly (L-lactic acid).

It has been confirmed that with a photoinitiator, it is possible for a monomer like polyacrylamide to either polymerize and form many short chains (like a brush) on the PLA polymer surface, or to polymerize into a few long chains attached to the PLA fibers. Due to time limitations, only the time variable was studied for the UV light initiated study, whereas for the UV/ozone irradiated samples, both the exposure time and the monomer concentration as well as experimental sequence were studied. Moreover, the uniformity of the collagen immobilized on the activated PLA surface was not very even and needs to be studied further.

CHAPTER 2 – REVIEW OF LITERATURE

2.1. Tissue Engineering

2.1.1. Background

Every year a large number of patients suffer from various diseases and need organ transplantation or implantation of medical devices ^[1]. Since the first organ transplantation performed by Murray and colleagues in 1954 ^[4], Transplantation technology has grown rapidly and different organs such as the pancreas, lung, heart and bladder have been transplanted successfully ^[5]. Taking heart disease as an example, over 8 million patients need transplantation every year in the United States ^[1].(Table 2.1)

Table 2.1. Cardiac procedures performed in the United States annually ^[5]

Indication	No. of Procedures
Angioplasty	926,000 (→ 539,000 PTCA)
Coronary artery bypass graft (CABG)	553,000
Valve replacement	89,000
Heart transplantation	2,340
Other open heart surgery	92,000

*PTCA = percutaneous transluminal coronary angioplasty

Indeed, transplantation plays a significant role in saving patients' lives. But the current situation is that the number of patients who need organ transplantation is growing at an alarming speed and it far exceeds the number of available organs. In 2001, the number of

patients who need transplantation was 74,800. After 5 years in 2006, the number had increased to 98,263. However, the actual number of patients who received transplanted organs was only 28,291 that year. This was only 28% of the demand ^[1].

Besides the shortage of available organs, there are other limitations to transplantation strategy, for example, the inflammatory response, the risk of infection during operation and the chance of rejection by the immune system are all contributing factors to clinical failure. So recently, more researchers are exploring the world of tissue engineering with the aim of “developing biological substitutes that restore, maintain, or improve tissue function” ^[1].

2.1.2. Definition

With increases in the human life span, people are seeking ways to repair or replace diseased tissues and organs. Tissue engineering or regenerative medicine is an innovative and interdisciplinary area that applies the knowledge of physics, chemistry, engineering and biology to develop materials for the improvement of biological functions and the replacement of organs ^[1]. The first recorded article using the concept of tissue engineering was called “Functional Organ Replacement: The New Technology of Tissue Engineering” ^[6]. It was published in 1991. Since that time the topic of tissue engineering has become increasingly popular and has been applied to the development of prosthetic devices and the surgical manipulation of tissues ^[7].

The approach of tissue engineering is first to understand tissue growth and then to develop substitutes for the replacement of malfunctioning tissues and organs [8]. During the last decade, it has made great progress and has been applied to a variety of tissues and organs, such as heart valves, kidneys, bladders and bones, ears and skins [9]. Figure 2.1 shows a schematic view of the steps in the tissue engineering approach.

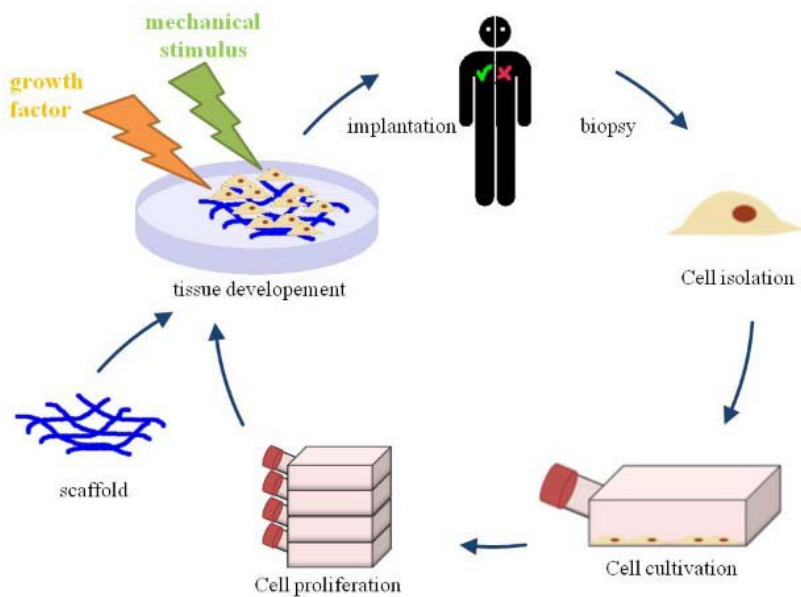


Figure 2.1. Basic approach to tissue engineering [8]

Firstly, cells should be isolated from the patient's body, and cultivated in vitro in the laboratory for proliferation and differentiation. Then, when there are enough cells, they can be seeded onto a porous polymeric scaffold and cultured in an incubator or bioreactor, where the scaffold is treated with mechanical stimuli and growth factors. Finally, it is implanted back in patient's body in the area of the tissue defect.

2.2. Scaffolds

2.2.1. Overview

Tissue engineering scaffolds are resorbable artificial and porous structures on which cells are seeded. They may be three-dimensional and inevitably have large surface area ^[10]. The main function is to provide a microenvironment and mechanical support for the transplanted or host cells to proliferate and differentiate. The design and fabrication of scaffolds is also an interdisciplinary challenge that requires researchers in computer science, material science, cell biology, mechanical engineering and immunology to collaborate and work together ^[11]. After the successfully regenerated of tissue has been accepted by the body, the scaffold has completed its mission and should degrade at a predictable rate. The preferred rate of degradation will depend on the type of cell, its rate of growth and the clinical application ^[12].

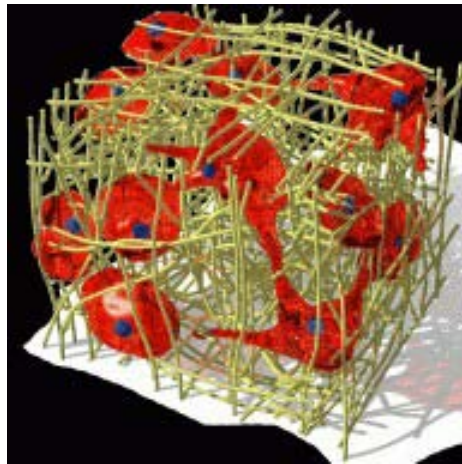


Figure 2.2. 3D image of a porous scaffold ^[13]

Figure 2.2 shows the 3D structure of a porous scaffold. From the image we can see that the cells can attach freely to the scaffold and have large room for growth and expansion. The main functions of the scaffold are listed as follows:

1. Allow cell attachment and migration;
2. Deliver and retain cells and biochemical factors;
3. Enable diffusion of vital cell nutrients and expressed products;
4. Exert certain mechanical forces and biological influences to modify the behavior of the cells.”^[8]

2.2.2. Materials

Many natural and synthetic biomaterials are being used to fabricate tissue engineering scaffolds for various applications. There are strict requirements for these materials since they are in direct contact with cells and the extracellular matrix (ECM). This means that the materials should:

1. Be biocompatible and biodegradable into nontoxic products;
2. Have a large surface area and porous structure, capable of being fabricated into the desired shape;
3. Promote cell adhesion, growth, proliferation and differentiation;
4. Have preferred mechanical properties^[14].

2.2.2.1. Natural Scaffolds

Natural polymers can mimic the extracellular environment better than synthetic polymers since they contain biological components. They are abundant in nature and are likely to have better biocompatibility and biodegradability ^[15]. Proteinic materials, such as collagen, fibrin, elastin and even gelatin, which is a partially degraded form of collagen, have all demonstrated their suitability as a desirable scaffold material.

Collagen is the one of the most popular natural polymers due to its abundance and superior biocompatible properties. It is the major component of the native extracellular matrix.

Currently, more than 20 different collagens have been identified ^[16,17]. Figure 2.3 shows the triple helix structure of collagen composed of three polypeptide chains. Collagen is arranged in fibrils, with a characteristic 67 nm axial periodicity ^[18].

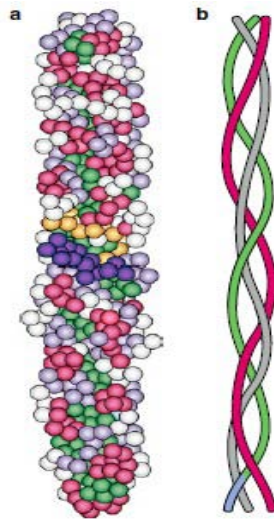


Figure 2.3. Structure of collagen (a) Model of collagen peptide. (b) Schematic of the triple helix ^[15]

Elastin is also a representative example of a natural polymer. Elastin has an isotropic, elastic structure that enables skin to return to its original shape and dimensions after it has been mechanically strained. Elastin is also a major structural protein found in the native extracellular matrix of connective tissues ^[11]. It has been selected as a preferred scaffold material because of its elasticity, ductility and biocompatibility. Its structure is illustrated in Figure 2.4.

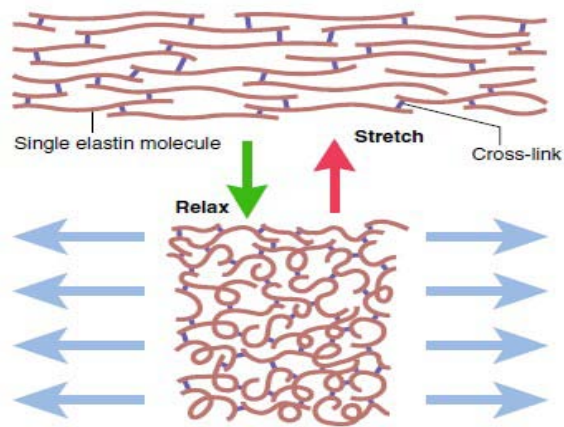


Figure 2.4. Elastin structure ^[15]

However, more research is needed to solve the common problems associated with natural polymers such as their inferior mechanical strength, inconsistent degradation time and the risk of a negative immune response ^[18].

2.2.2.2. Synthetic Scaffolds

Synthetic materials have several advantages over natural ones. For example, they are

relatively abundant, have superior mechanical properties and have degradation rates that are predictable, precise and well known. Researchers can select the synthetic material according to the specific requirements of the application ^[19]. Table 2.2 lists several popular polymers used for the fabrication of scaffolds.

Table 2.2 Properties of several synthetic polymers used for scaffolds ^[11]

Polymer	Degradation method	Degradation time	Primary degradation products	Bulk mechanical stiffness: E-modulus (GPa)	Tissue engineering applications
PGA	Ester hydrolysis	1–12 months	Glycolic acid	5–7	Skin, cartilage, bone, ligament, tendon, vessels, nerve, bladder, liver
PLA	Ester hydrolysis	5–60 months	Lactic acid	2–3	
PLGA	Ester hydrolysis	1–12 months	Lactic acid and glycolic acid	2–7	
PDO	Ester hydrolysis	3 weeks to 6 months		0.002–0.04	Orthopedics, drug delivery, bone, vessels
PCL	Ester hydrolysis	1–3 years	Caproic acid	0.4	Skin, cartilage, bone, ligament, tendon, vessels, nerve
PEG/PEO	Nondegradable	Not applicable	Not applicable	0.1–5	Drug delivery, cartilage

*PGA poly(glycolic acid); PLA poly(lactic acid); PLGA polylactide-co-glycolide; PCL polycaprolactone; PDO polydioxanone; PEG poly(ethylene glycol); PEO poly(ethylene oxide)

Take polylactic acid (PLA) as an example. This is an aliphatic polyester formed from the polymerization of lactide. As a result, it degrades by ester hydrolysis within the human body to form lactic acid which is easily eliminated from the body. It has 37% crystallinity, a glass transition temperature of 57–65 °C and a melting point of 150–160 °C ^[20,21]. Sterilization

process of this polymer may involve ethylene oxide or gamma radiation. If the later, care should be taken as over exposure to gamma radiation may cause chain degradation, cross-linking and a decrease in crystallinity ^[11]. Unlike PGA, PLA has a hydrophobic surface which needs to be modified in some way to facilitate wetting and cell adhesion.

However, there are still disadvantages associated with synthetic scaffolds. Compared to natural materials, synthetic polymers lack the biological component of the native ECM ^[22]. Some of the degradation products of these biodegradable polymers are not biocompatible, sometimes even cytotoxic, which can cause adverse reactions ^[23]. Therefore, scientists have been investigating ways of combining natural and synthetic materials together so as to create better performing scaffolds.

2.2.2.3. Multi-material Scaffolds

In order to overcome the disadvantages of both natural and synthetic polymers, some researchers are developing multi-material scaffolds. For example, Darling et al have successfully combine PCL, alginate and fibrin for better performance ^[24]. Zisch and Halstenberg are trying to develop synthetic materials that mimic the biological properties of natural polymers by incorporating the natural within the synthetic polymer RGD sequence ^{[25,}
^{26]}. These creative ideas and research represent attractive new strategies in the development of this field.

2.3. Surface Modification

2.3.1. Overview

Most materials do not meet the basic requirement of surface biocompatibility when implanted into the human body. This is important because it is biomaterials surface that first comes into contact with living cells and blood. Therefore, it is important to find an effective method to improve the biocompatibility by modifying the surface of the polymer for better biofunctionality while keeping the bulk properties constant. Actually, over the past 50 years synthetic materials have been subjected to surface modification. Table 2.3 shows a number of different methods for surface modification, including oxidation, coating, grafting and surface roughening. Some of these techniques are less suitable with polymeric materials or are used less often because of their high cost or environmental impact.

Table 2.3. General methods for surface modification ^[27]

	Examples
Roughening	Sand blast, etching
Oxidation	Alkaline treatment, chromium treatment, fire exposure, plasma treatment (glow and corona discharge)
Coating	Casting, lamination, plasma polymerization
Blending	Surfactant addition, block and graft copolymer addition
Ion implantation	High-energy argon and nitrogen injection
Graft polymerization	UV, ionizing radiation, low-temperature plasma

2.3.2. Concept of Surface Modification

The principle of polymer surface modification to enhance its biological performance is the same, regardless of the clinical application. Figure 2.5 shows the basic steps of this surface modification concept.

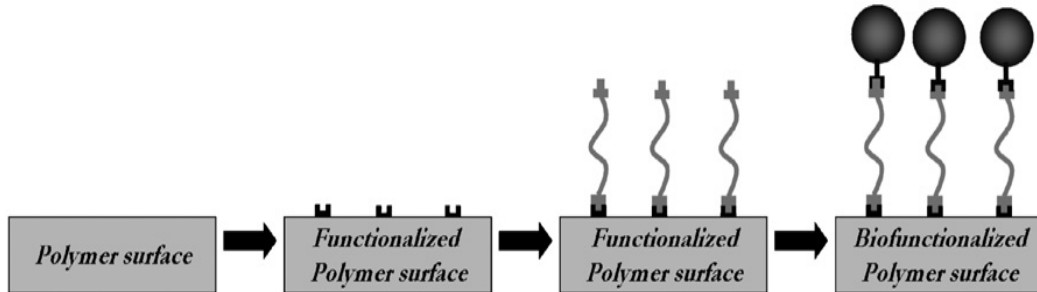


Figure 2.5. Concept of surface modification to improve biological properties ^[28]

Since many synthetic polymers are chemically inert, their surface must first be activated or functionalized before being able to attach any bioactive compounds. It is therefore important to determine the optimal type and quantity of functional groups to be attached to the polymer's surface. Then, as shown in Figure 2.5, a spacer molecule is introduced to improve the bioactivity and protein confirmation, and finally a bioactive compound is immersed on the modified polymer surface.

2.3.3. Techniques in Surface Modification

2.3.3.1. Ultraviolet Irradiation (UV)

Ultraviolet (UV) light has a wavelength of 10-400 nm which is invisible to the human eye. It can initiate chemical reactions and alter chemical bonds in polymers it is exposed to. It is also used to initiate radical graft polymerization, often in the presence of a photoinitiator or photosensitizer. Benzophenone (BP) has been used as an effective photoinitiator in recent research^[29,30]. BP is first excited to a singlet state, and then it jumps to a triplet state on exposure to UV light, as shown in Figure 2.6.

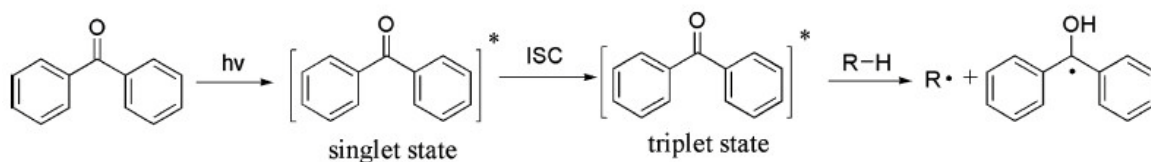


Figure 2.6. Photografting polymerization initiated by benzophenone^[30]

“BP in a triplet state undergoes hydrogen-abstracting reactions from substrates, then provides surface radicals ($\text{R}\cdot$) capable of initiating surface graft polymerization. The resulting benzopinacol radicals ($\text{BP-OH}\cdot$) are relatively less reactive and not prone to free radical polymerization, but tend to participate in termination by a coupling reaction.”^[31]

UV irradiation has been used to modify the surfaces of biomaterials to improve the biological properties. It provides a simple, low-cost and effective surface modification method.

2.3.3.2. Ultraviolet/Ozone Irradiation (UV/O₃)

Ultraviolet/Ozone (UV/O₃) irradiation has proven to be effective in cleaning surfaces by removing various kinds of contaminants ^[32]. It is also known to be a successful surface modification method, and is becoming increasingly popular because of its ability to use high radiation intensities compared to plasma treatments ^[33]. It can be conducted under atmospheric pressure and at low cost. Moreover, UV/O₃ is environmentally friendly, which means that it does not cause pollution. By exposing the material to UV light in an ozone atmosphere, the surface energy increases due to the breakdown of covalent bonds. However, the UV/O₃ has no negative effect on the bulk properties of the material ^[34].

2.3.3.3. Plasma Treatment

Radio frequency (RF) plasma treatment is a common way to modify the surface properties of various polymers ^[35]. Plasma is known as the fourth state of matter after solid, liquid and gas. It is composed of highly reactive molecules, ions and radicals which provide an excellent environment for competing chemical reactions at the surface ^[36]. The high concentrations of reactive species can etch the substrate with a uniform glow discharge at low temperature and so does not damage thermally sensitive substrates.

Atmospheric pressure plasma using a helium (He) or a He/O₂ atmosphere is now widely used to treat polymers in the biomedical field. Figure 2.7 shows a schematic diagram of

atmospheric pressure plasma jet applying toluene-tetraethoxysilane (TOES) and a helium/oxygen atmosphere.

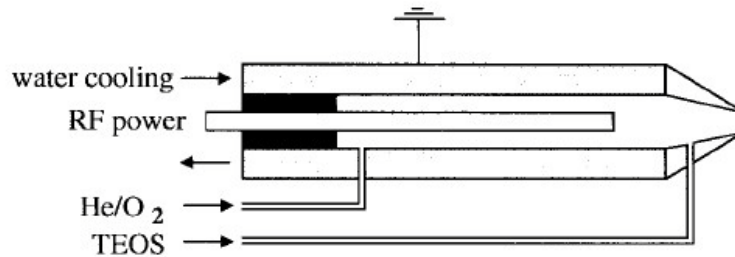


Figure 2.7. Schematic diagram of an atmospheric pressure plasma jet ^[37]

The plasma jet consists of two concentric electrodes and a mixture of helium and oxygen gas. The plasma gas discharge is ignited by applying a radio frequency potential to the inner electrode. Then the plasma gas is emitted from the nozzle and the active components are deposited onto the substrate for surface modification.

There are also many parameters, such as gas composition, plasma treatment time and radio frequency, which should be taken into account when treating a specific material ^[38]. Figure 2.8 lists some common plasma parameters. Usually the parameters of the substrate and reactor are predefined, because the result of plasma treatment is dependent on the plasma intensity, the gas flow and other related conditions. A series of preliminary trials should be undertaken in order to achieve the optimum conditions.

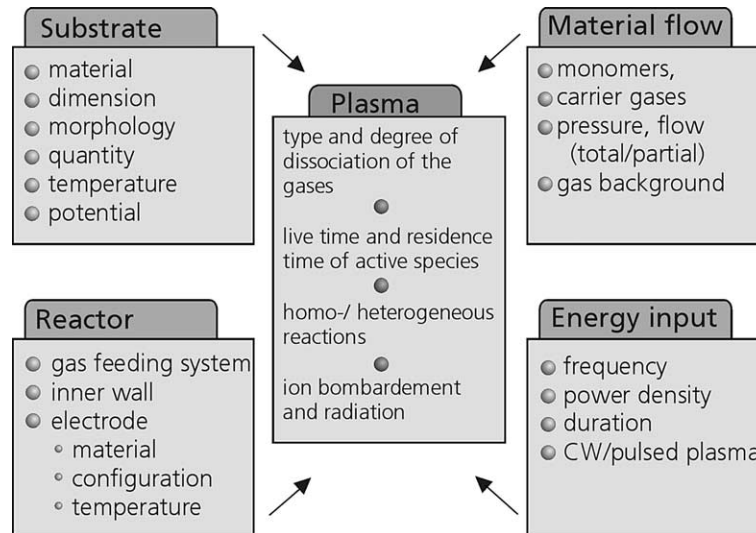


Figure 2.8. Plasma parameters ^[38]

However, there is a disadvantage of plasma treatment that cannot be ignored. This is the aging effect. The active species created by the plasma on the surface of the substrate tend to react with the ambient atmosphere and tend to disappear with time. This is an important factor because the need to immobilized biocompatible molecules on the activated surface should occur in a rapid and reliable manner. By delaying the biofunctionalization, the modified surface will not give consistent clinical results.

2.4. Immobilization of Bioactive Compounds

When a scaffold is implanted in the human body, the surface of the scaffold will first come into contact with blood proteins and cells. A limitation faced by most biodegradable materials is their lack of biocompatibility and biostability. In many cases, the surface of the

polymer is hydrophobic and cell-material interactions are limited. Therefore it is important to immobilize certain bioactive compounds such as protein and peptides to the polymer surface where cells can bind, grow and proliferate^[39]. The immobilization of protein macromolecules on a chemically inert polymer surface could be done through physical methods or chemical methods using carbodiimide or sulfonyl chloride chemistry^[40, 41].

Collagen, one of the most important and abundant components of extracellular matrix in the human body, is biodegradable and biocompatible and comprises up to 30% of the total amount of protein in the human body. Since cells are surrounded by extracellular matrix, collagen has been successfully immobilized onto scaffold surfaces for tissue engineering applications^[42]. Figure 2.9 shows a schematic diagram of the collagen fibril structure.

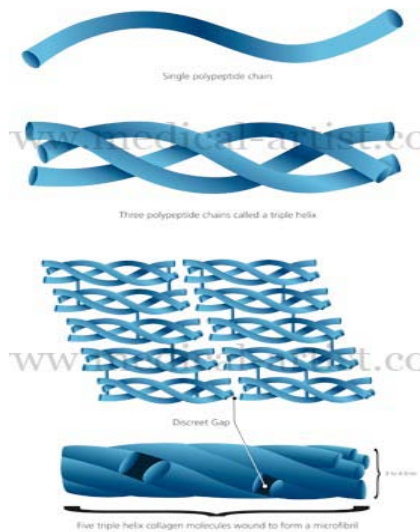


Figure 2.9. Schematic diagram of collagen fibril structure^[43]

The structure of collagen fibrils consists of three single polypeptide chains wound together to form a triple helix. Then five triple helix collagen molecules wind around each other to form a microfibril. These collagen microfibrils pack together to form bundles of a higher order.

There are a number of ways to attach bioactive compounds such as collagen to the surface of a scaffold. A variety of linking agents or spacer molecules have been investigated to link the bioactive compounds to the scaffold substrate^[28]. One of the most frequently used crosslinking agent is glutaraldehyde^[44]. However, the toxicity of glutaraldehyde has proven hazardous to cells and tissue^[45,46]. So recently some natural crosslinking agents have been studied, such as genipin^[47].

Genipin is obtained from its parent compound geniposide derived from the fruit of *Gardenia jasminoides*. It is relatively abundant^[47]. Compared to glutaraldehyde, genipin has better cytocompatibility and causes less inflammation and calcification. Genipin is an excellent and effective natural crosslinking agent for proteins. At the same time, it serves as a spacer molecule enabling collagen or other proteins to move and orientate more freely so as to achieve a preferred conformation and provide better function in the biological environment.

2.5. Surface Characterization Methods

Surface characterization methods are used to study how different surface modifications change the properties of the polymer's surface. In this part, some of the more common

characterization methods are introduced, including a description of their principles, functions and applications.

2.5.1. Fourier Transform Infrared Spectroscopy (FTIR)

Fourier transform infrared spectroscopy (FTIR) is a technique used to obtain an infrared absorption spectrum, from a liquid, gas, powder or film. An FTIR spectrometer collects relative absorption data over a whole IR spectral range from 600-4000 cm^{-1} [48]. When the data is collected, a Fourier transform is needed to convert the raw data into the actual spectrum for further analysis.

Infrared spectroscopy can probe the molecular vibrations of different functional groups since each group has a different vibrational frequency. As a result, each group is associated with a different infrared absorption band [49]. Below Table 2.4 lists the absorption frequencies of the most commonly found chemical bonds and groups.

Table 2.4. Common infrared absorption frequencies ^[50]

CHARACTERISTIC INFRARED ABSORPTION FREQUENCIES		
Bond	Compound type	Frequency range cm ⁻¹
C—H	Alkanes	2850–2960
		1350–1470
C—H	Alkenes	3020–3080
		675–1000
C—H	Aromatic rings	3000–3100
		675–870
C—H	Alkynes	3300
C=C	Alkenes	1640–1680
C≡C	Alkynes	2100–2260
C=C	Aromatic rings	1500, 1600
C—O	Alcohols, ethers, carboxylic acids, esters	1080–1300
C=O	Aldehydes, ketones, carboxylic acids, esters	1690–1760
O—H	Monomeric alcohols, phenols	3610–3640
	Hydrogen-bonded alcohols, phenols	3200–3600
	Carboxylic acids	2500–3000
N—H	Amines	3300–3500
C—N	Amines	1180–1360
C≡N	Nitriles	2210–2260
—NO ₂	Nitro compounds	1515–1560
		1345–1385

An FTIR spectrometer with an attenuated total reflectance (ATR) attachment is the preferred method for controlling the sampling depth and resolution of thin solid samples. It is also popular because samples can be tested directly without complicated preparation procedures ^[51]. Figure 2.10 illustrates the principles of the ATR system. The sample is placed against the flat crystal surface. Then the infrared beam undergoes multiple internal reflections as it passes through the inside of the crystal of high refractive index at a certain angle of incidence. This internal reflectance creates an evanescent wave that goes through the sample and is

attenuated wherever the sample absorbs energy. Then the attenuated energy is passed to the detector of the infrared spectrometer. That is basically how the ATR system generates the spectrum of a sample ^[52].

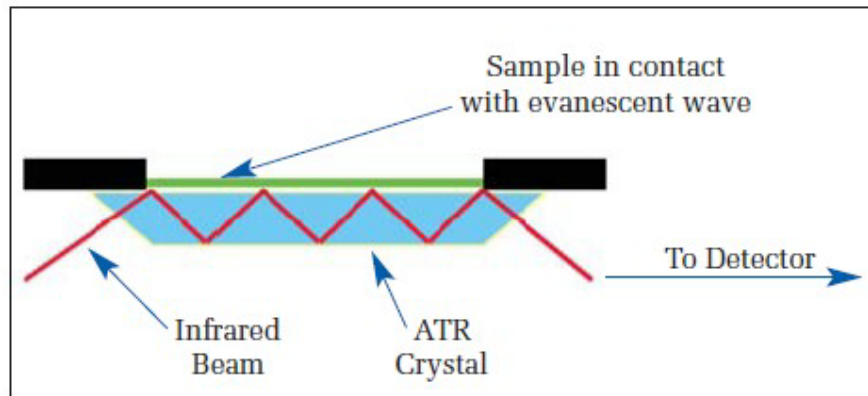


Figure 2.10. Principle of ATR system ^[52]

FTIR spectroscopy has a wide range of applications such as in food analysis and gas and solid surface analysis. Recently, it has been applied to the field of biomedical research for the analysis of cells and tissues. In this research project, FTIR-ATR spectroscopy is used to determine the extent and type of chemical modification of the fiber surfaces caused by the treatments.

2.5.2. Water Contact Angle Analysis

Wettability is an important surface property for textile fabrics. It is associated with intermolecular interactions at the liquid, vapor and solid interfaces. The wettability of a

surface is defined as the contact angle between a droplet of the liquid in thermal equilibrium with a horizontal surface. A schematic view is shown in Figure 2.11.

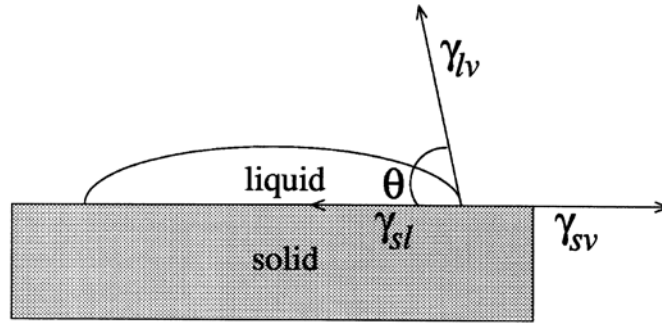


Figure 2.11. Contact angle of a liquid droplet onto a solid surface ^[53]

The contact angle is easily measured by calculating the tangent of the angle (θ) between the edge of the liquid drop and the solid surface. It is defined by the mechanical equilibrium of the drop under the action of three interfacial tensions: solid-vapor, γ_{sv} , solid-liquid, γ_{sl} , and liquid-vapor, γ_{lv} . This equilibrium relation is known as Young's Equation with the assumption that the solid surface is smooth, rigid and chemically inert to the liquid.

Meanwhile, the liquid should not be physically absorbed by the solid substrate. Here is

Young's equation derived by Thomas Young in 1805 ^[53]:

$$\gamma_{lv} \cos\theta_Y = \gamma_{sv} - \gamma_{sl} \tag{1}$$

where θ_Y is the Young contact angle.

Table 2.5 lists different ranges of contact angles and classifies their solid/liquid and

liquid/liquid interactions. Generally, water is the liquid used for analysis. When the contact angle is below 90° , the surface can be termed hydrophilic. For contact angles between 90° and 180° , the surface is hydrophobic. And for those between 150° and 180° , the surface can be defined as superhydrophobic.

Table 2.5 Typical contact angle values ^[54]

Contact angle	Degree of wetting	Strength of:	
		Solid/liquid interactions	Liquid/liquid interactions
$\theta = 0$	Perfect wetting	strong	weak
$0 < \theta < 90^\circ$	high wettability	strong	strong
		weak	weak
$90^\circ \leq \theta < 180^\circ$	low wettability	weak	strong
$\theta = 180^\circ$	perfectly non-wetting	weak	strong

2.5.3. Scanning Electron Microscopy (SEM)

A scanning electron microscope (SEM) is a microscope that uses an electron beam instead of visible light to capture images of the surface topography of samples. It has a history of more than 75 years since Max Knoll first obtains SEM images in 1935 ^[55]. SEM can provide detailed information about the microstructure, surface morphology and composition of a sample.

SEM has been applied to many areas related to surface and material science, such as polymers, fibers and textiles, medicine, biology and tissue engineering. It has several

advantages compared to optical microscopy. For example, it has high resolution so the images are enlarged, clearly defined and have a large depth of field. SEM also has a wide range of magnifications from 10 to 500,000 times which can be altered and controlled according to the specific viewing requirements. However, sample preparation and the operation of the instrument are unique to SEM and need to be learnt prior to use.

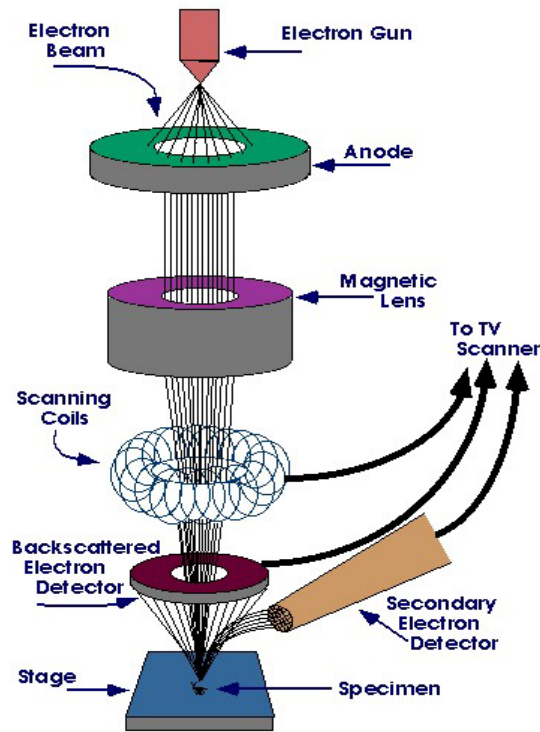


Figure 2.12. Schematic view of SEM ^[56]

Figure 2.12 presents a schematic view showing how an SEM works. In summary, an electron beam is emitted from an electron gun at the top of the column. The electron beam is focused by a condenser lens and passes through scanning coils. When the primary electron beam hits the gold or platinum coated specimen mounted on the stage, the electrons lose energy. This

results in the emission of secondary electrons and backscattered electrons (Figure 2.13). They are detected by a secondary electron detector and a backscattered electron detector, respectively. All the signals are then collected, amplified and transferred to a computer. Finally, a distribution map of the intensity of the various signals is created by the software, and it becomes the SEM image ^[57].

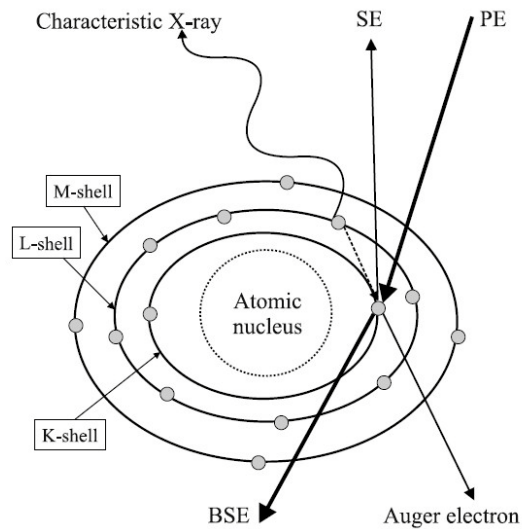


Figure 2.13. Inelastic interaction between primary electrons and those in atomic shells^[57]

*PE-Primary electron; SE-Secondary electron; BSE-Backscattered electron

If the primary electrons have enough energy, when they hit the sample surface, they can produce different signals, such as secondary electrons, backscattered electrons, characteristic X-rays, auger electrons, photons, visible light and. Then different detectors collect these X-rays, secondary electrons, backscattered electrons and convert them into an image showing the signal intensity distribution ^[57].

2.5.4. X-ray Photoelectron Spectroscopy (XPS)

X-ray photoelectron spectroscopy (XPS) is a surface chemical analysis technique and is sensitive to different elements located at the surface. It can be used to measure the elemental composition, electronic and binding states of the elements, oxidation numbers and the functionality of the solid material surface. XPS operates by irradiating the sample with a beam of x-ray photons which penetrate the sample surface to a depth of between 1 to 10 nm. The high energy x-rays interact with the atoms on the surface causing electron emission by a photoelectric effect.

Since the energy of the irradiated x-ray is already known, the electron binding energy (BE) of each emitted electron can be determined by the photo-chemical quantum equivalent law derived and explained by Einstein in 1905 ^[58]:

$$h\nu = E_{\text{binding}} + E_{\text{kinetic}} + \Phi \quad (2)$$

where E_{binding} is the binding energy (BE) of the electron, E_{kinetic} is the kinetic energy of the electron as measured by the instrument, ϕ is the work function of the spectrometer, ν is the frequency of the x-ray photons being irradiated and h is Planck's constant ^[59].

Binding energy is the energy difference between the initial and final states. It can be used to identify and determine the type and concentration of the elements at the surface since each element has a unique binding energy. Therefore, XPS must be performed under ultra high

vacuum (UHV) conditions for accuracy of electron counting. Below is Figure 2.14 showing the basic components of an XPS system and how they function together.

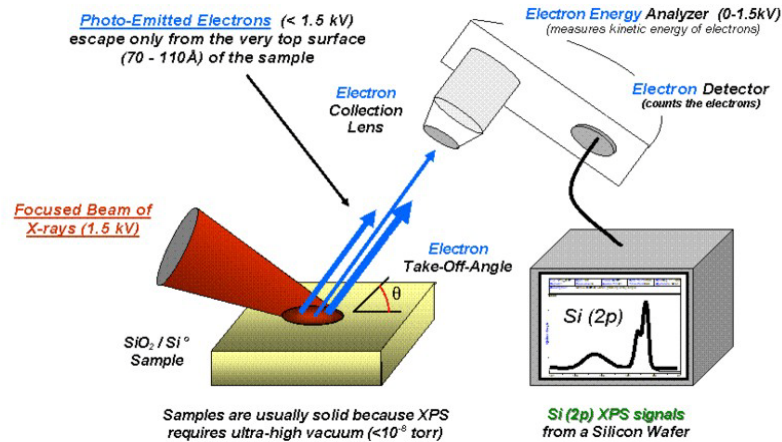


Figure 2.14. Components of a typical XPS system [60]

2.5.5. Time-of-flight Secondary Ion Mass Spectrometry (TOF-SIMS)

Time-of-Flight Secondary Ion Mass Spectrometry (TOF-SIMS) [59] is another sensitive surface analytical technique for acquisition of elemental and molecular information from the surface (top 10 to 20 Å) of a material with high spatial and mass resolution. TOF-SIMS can provide information such as chemical composition, distribution of chemical species and depth profiling.

The principle of TOF-SIMS is shown in Figure 2.15. A finely focused, pulsed primary ion beam is rastered across the surface of the sample and the secondary ions emitted at each irradiated point are accelerated into a time of flight mass spectrometer. In this way, an image

with sub micrometer ($< 0.3\mu\text{m}$) spatial resolution can be acquired with a full mass spectrum of ionic species for each pixel.

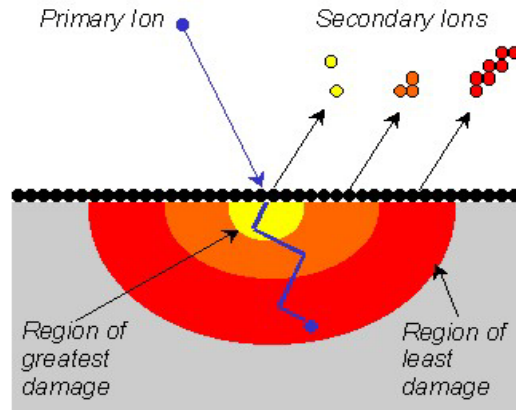


Figure 2.15. Schematic diagram of the SIMS process ^[62]

The total accumulated primary ion dose required to generate a spectrum by image acquisition is less than 1×10^{13} ions/cm², a concentration of ions which is within the static SIMS regime.

The static SIMS condition dictates that less than 1% of the sample surface should be impacted by the primary ion beam during a sample analysis so as to ensure that ejected secondary ions originate from an undamaged portion of the surface. Secondary ions were extracted into a TOF mass spectrometer with post acceleration to improve detection sensitivity. By combining a specific primary ion pulse width with a tuned TOF analyzer, it is possible to provide a mass resolution of approximately 5000m/Dm at 29AMU. The positive secondary ion mass spectra are calibrated using H⁺, C⁺, CH⁺, CH₂⁺, C₂H₅⁺ and C₃H₇⁺, while the negative secondary ion mass spectra are calibrated using C⁻, O⁻, OH⁻ and Cn⁻.

CHAPTER 3—EXPERIMENTAL

3.1 Approach of this research

The approach taken by this research study has been to search for the optimal effectiveness of different surface modification techniques such as UV, UV/ozone irradiation and plasma treatment for PLA nonwoven fabrics. Acrylamide was used as the monomer to activate the surface of PLA fibers by means of a graft polymerization technique. Different parameters like irradiation time, irradiation intensity, process sequence, monomer concentration were varied in the study so as to find the optimal conditions for polymerization. Then a natural crosslinking agent, genipin, was introduced to serve as a spacer molecule. After genipin was attached, collagen was applied to the surface to improve the biocompatibility and cell viability.

3.2 Materials

3.2.1 PLA fabric

Poly(lactic acid) (acid) is one of the most extensively used biodegradable polymers with a chemical structure shown in Figure 3.1. From the structure it is easy to tell that PLA is a relatively hydrophobic polymer.

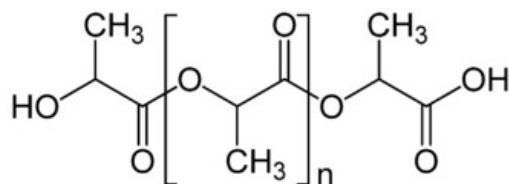


Figure 3.1. Chemical structure of PLA

Polylactic acid (PLA) nonwoven fabric was obtained from Ahlstrom Nonwovens LLC which is located at Windsor Locks, CT. The bonded web had been needle punched and had a basis weight of 20 gsm. Following are some thermal properties of the PLA fabric provided by the company in Table 3.1:

Table 3.1. Thermal properties of the PLA as provided by Ahlstrom Nonwovens LLC

Property	Temperature (°C)
Glass transition temperature	64
Melting point	164

It is believed that this PLA nonwoven web had been manufactured from a poly (L-lactic acid) resin synthesized with <2% D-isomer as a thermoplastic fiber forming polymer (Nature Works LLC, Minnetonka, MN) with a specific gravity of 1.24g/cm³.

Since there was dirt and contaminants on the fabric surface, the PLA fabric was scoured upon arrival in Pilot Laboratory using a non-ionic surfactant (Triton X-100) at 60 °C for 20 minutes and then rinsed with deionized water. After scouring, the samples were dried in a vacuum oven at 50 °C over night and then were stored in sealed paper envelopes. All samples are stored in a vacuumed desiccator prior to further treatment. An optical and an SEM image of the scoured PLA are shown in Figure 3.2.



(a)

(b)

Figure 3.2. (a) Optical image of scoured nonwoven PLA fabric; (b) SEM image of scoured nonwoven PLA fabric

3.2.2 Acrylamide

The monomer acrylamide has previously been successfully immobilized onto chemically inert polymeric substrates such polyethylene terephthalate (PET) [63]. In this way surface activation can be readily achieved by grafting reactive functional groups onto an inert substrate material. Acrylamide has a chemical formula of C_3H_5NO whose chemical structure is shown in Figure 3.3. It was obtained from Sigma Aldrich with purity of 99+%.

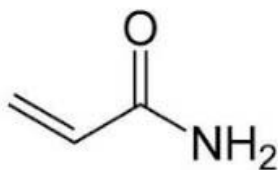


Figure 3.3. Chemical structure of acrylamide

3.2.3 Potassium persulfate

Polymerization of acrylamide was initiated by the generation of free radicals from potassium persulfate, which took on an important role as a thermal initiator. Potassium persulfate is used together with acrylamide to start the process of polymerization under UV/Ozone and plasma treatment. It was obtained from Sigma Aldrich with purity of 99+% and has a chemical formula of $K_2S_2O_8$.

3.2.4 Benzophenone

Benzophenone served as a photo initiator for UV polymerization. It can be used to initiate radical graft polymerization and has proven to be effective in recent researches) ^[63].

Benzophenone was obtained from Sigma Aldrich with purity of 99+% and its chemical structure is shown in Figure 3.4.

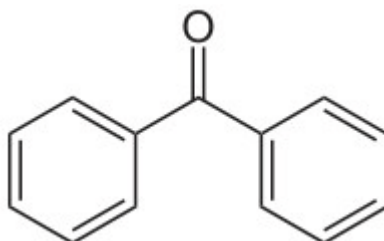


Figure 3.4. Chemical structure of benzophenone

3.2.5 Genipin

Genipin has recently been used as a natural crosslinking agent for tissue, chitosan and collagen ^[64]. Studies have identified that genipin can serve as a spacer molecule and be

utilized to crosslink functional amine groups present in natural tissues with little cytotoxic effects^[64]. Genipin is obtained from Wako Chemicals with purity of 98+%, and the chemical structure of genipin is shown in Figure 3.5.

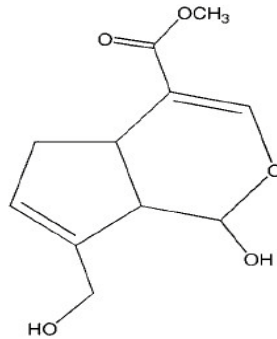


Figure 3.5. Chemical structure of genipin

3.2.6 Collagen

Being the most abundant protein in mammals, collagen is well known and recognized as a major component in extra cellular matrix where it promotes cell attachment, growth and proliferation. In this research, Type I collagen obtained from calfskin was supplied by MP Biomedicals LLC. It was immobilized to the activated PLA nonwoven fabric, through the genipin spacer molecule.

3.3 Experimental Methods

3.3.1. Surface modification

Because PLA is a chemically inert polymer, it has few reactive groups. Even though it has high biocompatibility, it is difficult to attach bioactive compounds to its surface. In this

research, three different surface modification methods were studied to experimentally graft some chemically active sites such as amino groups, to the PLA surface. These three methods were UV/Ozone irradiation, plasma treatment and UV irradiation. Acrylamide was selected as the monomer to be polymerized and potassium persulfate and benzophenone were the initiators in the polymerization process. The goal was to maximize the extent of polymerization of acrylamide on the surface.

3.3.1.1 UV/ozone (UVO) polymerization

In this part, UV/ozone (ultraviolet ozone) irradiation was used to promote acrylamide to polymerize on the PLA fabric's surface. Figure 3.6 shows the UVO system (Model T10X10/OES) from UVOCS which is located in Lansdale, PA. This system was generously provided by Dr. Willoughby and her research group. The main part of UVOCS equipment is a low-pressure quartz mercury vapor lamp, which generates UV emissions in the 254 and 185 nanometer range. Ozone and atomic oxygen are generated. So the chemical bonds in the PLA polymer chain can be activated which leads to acrylamide attachment.



(a)

(b)

Figure 3.6. UVO source. (a) UVOCS system; (b) PLA samples to be irradiated

To achieve the optimal surface treatment condition for the PLA samples, several different approaches regarding sequence, irradiation time and monomer concentration were attempted.

Approach 1

One PLA fabric sample was taken out of the sealed envelope and placed directly in the UVO chamber and irradiated for 5 minutes. After being treated, the PLA fabric swatch was immersed in an aqueous solution of potassium persulfate (0.15 mol/L), and acrylamide (1 mol/L) at room temperature for two hours. A second PLA sample was then taken out and first immersed in an aqueous solution of same chemical components and concentrations for two hours. Then the sample was dried in a hot air oven at 50 degree C for 30 minutes and then put in a desiccator overnight. After these steps, it was treated with UV/ozone irradiation

for 5 minutes. A control sample was kept for comparison. It was neither immersed in the solution nor irradiated with UV/ozone.

All three samples were rinsed with copious amounts of deionized water to remove any ungrafted monomer present on but not attached to the surface. Then the samples were dried in the oven at 50 degree C for 30 minutes and kept in a vacuum desiccator for 48 hours to reach a constant weight. They are then sealed in paper envelopes prior to further analysis.

Approach 2

This approach aimed to determine the effect of treatment time of UV/ozone exposure on the extent of surface modification. The following irradiation times: 1 min, 2min, 3 min, 5 min, 10min and 15min, were varied while the other variables were kept constant. A control sample with 0min irradiation was taken for comparison.

The PLA fabric swatches were taken out of their sealed envelopes and immersed in an aqueous solution of potassium persulfate (0.15mol/L), and acrylamide (1 mol/L) for two hours (pH~9, 23-25C). All the samples were dried in a hot air oven for half an hour at 50 degree C and put into a vacuum desiccator overnight. Then they were treated with UV/O₃ irradiation for 1 min, 2min, 3 min, 5 min, 10min and 15min, respectively. After the irradiation step, the fabrics were rinsed with copious amounts of deionized water to remove any ungrafted monomer present on but not attached to the surface. Then the samples were dried in the oven at 50 degree C for 30 minutes and put into a vacuum desiccator for 48 hours to reach a constant weight. They were then sealed in paper envelopes for further analysis.

Approach 3

In this third approach we determine how the extent of polymerization varied with monomer concentration. We set 4 levels of monomer concentrations from 0 to 1 mol/L at interval of 0.33mol/L.

The PLA fabric swatches were taken out of their sealed envelopes and immersed in an aqueous solution of potassium persulfate (0.15 mol/L), and acrylamide which varied from 0mol/L, 0.33 mol/L, 0.67 mol/L, and 1 mol/L at room temperature for 2 hours. All samples were dried in the oven at 50 degree C for 30 minutes and dried in a vacuum desiccator overnight. Then the samples with different monomer concentrations were irradiated under UV/ozone for 5 min. After the irradiation step, the samples were rinsed with copious amounts of deionized water to remove any ungrafted monomer present on but not attached to the surface. Then the samples were dried in a hot air oven at 50 degree C for 30 minutes and stored in a desiccator for 48 hours so as to reach a constant weight prior to being sealed in paper envelopes for further analysis.

3.3.1.2 Plasma polymerization

An atmospheric pressure plasma jet (APPR) machine with radio frequency (RF) power was used to evaluate the polymerization rate of acrylamide on PLA fabric under RF plasma conditions. Figure 3.7 shows the plasma source provided for use by Dr. El-Shafei.



Figure 3.7. Atmospheric pressure plasma jet (APPR)

As Figure 3.6 shows, the sample loading area was a flat stage where the samples were mounted using double-sided tape to keep them stationary for the treatment. Gas flow rates were set at 40 L/min. The distance between the stage and the electrode was 3 mm. Once the chamber was filled with the gas, the RF plasma was generated and the samples were treated. After plasma exposure for a certain period of time, the power lever was turned down and the sample could be removed from the chamber.

Helium and argon are commonly used noble gas in order to keep the discharge stable. It is also possible to add a little percent of oxygen which provides active species to the plasma system. However, when oxygen is added to the system, the plasma intensity is reduced to about 400W. Only with a 100% helium environment can the plasma intensity reach 800W.

To compare different plasma treatment conditions for the PLA samples, there were several variables such as plasma intensity, plasma gas type, exposure time and monomer concentration that needed to be evaluated independently.

PLA fabrics were immersed in aqueous solutions of potassium persulfate (0.15 mol/L), and acrylamide (1 mol/L) for 2 hours at room temperature. Then the samples were dried in the oven at 50 degree C for 30 minutes and placed in a vacuum desiccator overnight. Then the fabric was treated by one of the following three plasma sets of conditions.

1. Plasma intensity – 400W and 800W;
2. Plasma gas type – pure helium and helium mixed with small amount of oxygen (99.5% + 0.5%);
3. Plasma treatment time – 1 min, 2min, 5 min.

After the plasma treatments, the samples were rinsed with copious amounts of deionized water to remove any ungrafted monomer that did not adhere to the surface. Then the samples were dried in a hot air oven at 50 degree C for 30 minutes and put into a desiccator for 48 hours prior to reaching a constant weight. They were then stored in paper envelopes prior to further analysis.

To study how monomer concentration affects the extent of polymerization, monomer solutions of acrylamide were prepared beforehand at four concentrations from 0 mol/L to 1 mol/L at intervals of 0.33 mol/L. After immersing and drying, the samples were treated in helium plasma at 800W for 1 min, 2min and 5 min.

After the plasma treatment, the samples were rinsed with copious amounts of deionized water to remove any ungrafted monomer or unattached polymer still present on the surface. Then the samples were dried in the oven at 50 degree C for 30 minutes and put into a vacuum

desiccator for 48 hours to reach a constant weight. They were then sealed in paper envelopes for further analysis.

3.3.1.3 UV polymerization

A UV source from Spectrolinics Corporation (Model number ENF-240C) was included in this research to study the extent of acrylamide polymerization rate on PLA fabric. Figure 3.8 shows the UV source provided by Dr. Willoughby.



Figure 3.8 UV source

First the PLA nonwoven fabric was immersed in an ethanol solution of benzophenone (BP), the photoinitiator (0.055 mol/L) and the monomer acrylamide (1 mol/L) at 25 degree C for 2 hours. Then the samples were taken out, dried in the oven at 50 degree C for 30 minutes and put into a vacuum desiccator overnight. The fabric was then exposed to UV irradiation ($\lambda=365$ nm) for either 1, 2, or 5 min. The wavelength at 365nm was selected since it belongs

to the range where the photoinitiator is activated and the mechanism of radical polymerization is catalyzed. After polymerization, the PLA sample was rinsed with copious amounts of deionized water to remove any ungrafted monomer or unattached homopolymer still present on the surface. Then the samples were dried in the oven at 50 degree C for 30 minutes and put into the vacuum desiccator for 48 hours to reach a constant weight. They were then sealed in paper envelopes for further analysis.

3.3.2. Genipin attachment

A 40mmol/L genipin solution was made by dissolving 0.18 g of genipin powder in 20mL of PBS buffer at pH 7.4. The dissolution process took place in a shaker bath at 60 rpm and 37 degree C for about three hours. When the genipin solution became transparent, the functionalized PLA sample was immersed in the genipin solution to affect the cross linking reaction in sealed glass vials.

After the reaction, the sample was taken out and rinsed with copious amount of deionized water to remove excess genipin from the surface. Then the samples were air dried and put in the vacuum desiccator for 48 hours to reach a constant weight. They were then sealed in paper envelopes for further analysis.

3.3.3 Collagen immobilization

A 0.01% collagen solution was prepared using 0.1M acetic acid (Fisher Scientific) for dissolution at room temperature. The 0.1M acetic acid solution was prepared by dissolving

5.72ml acetic acid in 994.28ml deionized water. Then the collagen solution was prepared by diluting 0.1% collagen solution (Sigma Aldrich) to a working concentration of 0.01% using the acetic acid. Once the solution was prepared, the genipin treated samples were immersed in the collagen solution and left overnight at 2-8°C in the refrigerator to allow the protein to bind to the surface. The collagen immobilized PLA samples were then removed from the collagen solution and thoroughly washed in copious amounts of deionized water to remove any unattached collagen from the fiber surface.

3.4 Analysis

3.4.1. Fabric thickness measurement

The thickness of the PLA fabrics before and after surface activation and functionalization was recorded in order to observe the extent of monomer polymerization from a macroscopic point of view.

The thickness measurements were performed using a SDL thickness gauge. Three readings were taken from different areas of the samples which were selected at random. They were used to calculate the sample average value.

3.4.2 Surface analysis

This section discussed some of the techniques of surface analysis and how these techniques are used to analyze the surface chemistry.

3.4.2.1 Contact angle measurements

The wettability of a fabric can be measured by a contact angle test. It provides information about the hydrophilic or hydrophobic nature of the fabric and it also can be used to determine the surface energy of the fabric.



Figure 3.9. OCA 20 DataPhysics optical contact angle measuring system

The contact angle test was performed on a Model OCA 20 DataPhysics video-based optical contact angle measuring system as shown in Figure 3.9. The software used was SCA 20. The instrument was equipped with a CCD video camera with a resolution of 768 x 576 pixels, an electronic dosing system, an electrically driven sample stage and a syringe. The PLA samples were cut to a size of 1 cm x 4 cm rectangle and taped onto the stage. A 500 μ L syringe was filled with distilled water and fixed to the dosing system. Then SCA 20 software was turned on for parameters adjustment. The drop size was set as 5 μ L and dropping rate of 10 μ L/min.

Sample stage was adjusted to make sure that needle and sample were both clear shown in the video. The water droplet was then dispensed onto the fabric and remained for 20 s before measuring the contact angle with the software. For each sample, at least five measurements were taken from different surface locations selected at random. The mean and standard deviation were then calculated.

3.4.2.2 Fourier transform infrared (FTIR) spectroscopy

FTIR spectroscopy is an effective way to observe the chemical characteristics of a fiber surface. The interaction between infrared light and the vibrational motion of the covalent chemical bonds is recorded on an absorption spectrum.

The FTIR spectrometer used in this research was the Thermo Nicolet Nexus 470 as shown in Figure 3.10. It was located in the Analytical Lab, College of Textiles. The software for this equipment is Omnic version 7.2.



Figure 3.10. FTIR equipment

An attenuated total reflectance (ATR) attachment was involved in this equipment. The infrared radiation went through an infrared transmitting germanium crystal which had a high refractive index in order to generate multiple internal reflections along the sample surface.

The parameters used in this research are as follows:

Number of scans: 32

Resolution: 4 cm^{-1}

Range: $4000 - 700\text{ cm}^{-1}$

Final format: Absorbance

The germanium crystal was cleaned with methanol and background spectrum was collected each time before a sample spectrum was collected. The fabric sample was first cut to a size of $5\text{mm} \times 10\text{mm}$. It was then folded to double its thickness and mounted onto the crystal for improved absorbance. Thirty two scans of the spectrum were collected for further analysis.

Wavenumbers at each peak were marked to identify the specific chemical groups and bonds.

By comparing the chemical peaks of different samples, it was possible to detect any chemical changes that occurred to the surface of PLA fabrics.

3.4.2.3. X-ray photoelectron spectroscopy (XPS)

X-Ray Photoelectron Spectroscopy (XPS) is capable of analyzing the top surface layer of a sample. Elemental identification of the surface can be achieved with about 0.1% atomic detection limit. From these scans, information about the chemical state of each element can

be obtained, and any changes of the chemical content cause by surface modification can be detected. Figure 3.11 below shows the SPECS XPS instrument in the Surface Analysis Laboratory, MRC Building. A monochromatic x-ray source was located perpendicular to the hemispherical analyzer PHOIBIS 150. The X-Ray incidence angle was set at about 30° and x-ray source to analyzer angle was about 60°. Energy calibration was established by referencing to adventitious carbon (C1s line at 285.0 eV binding energy). The samples were kept overnight under vacuum after conditioning in a vacuum chamber at which the pressure was held in the 10⁻¹⁰ mbar range.

The samples were sent to the Analytical Instrumentation Facility for testing. Results were recorded as Excel files. Further analysis was done using XPSpeak software.



Figure 3.11. XPS system (Image courtesy of Analytical Instrumentation Facility, NCSU)

3.4.2.4. Time-of-flight secondary ion mass spectrometry (TOF-SIMS)

TOF-SIMS spectrometry were performed using TOF-SIMS V (ION TOF, Inc. Chestnut Ridge, NY) instrument equipped with a Bi_n^{m+} ($n = 1 - 5, m = 1, 2$) liquid metal ion gun. The instrument's vacuum system consisted of a load lock for sample loading and an analysis chamber, separated by a gate valve. The analysis chamber pressure was maintained below 5.0×10^{-9} mbar to avoid contamination of the surfaces to be analyzed. For the high mass resolution spectra acquired in this study, a 128 by 128 pixel spectrum of a $100 \mu\text{m}$ by $100 \mu\text{m}$ area was acquired using the Bi^+ primary ion beam. For the mass spectral images, a 256 by 256 pixel image of a $200 \mu\text{m}$ by $200 \mu\text{m}$ area or a $500 \mu\text{m}$ by $500 \mu\text{m}$ area was acquired using Bi_3^+ primary ion beam^[65].

Samples for TOF-SIMS analysis were cut into $1\text{cm} \times 1\text{cm}$ size squares. Several different methods of recording TOF-SIMS data were used in this research: 1) The signal intensities for different mass per charge ratios were evaluated and plotted for each sample; 2) Characteristic peaks were recorded for comparison between samples; 3) Mapping technique of TOF-SIMS data was used to provide an image of the distribution and uniformity of the collagen immobilized on the PLA fabric sample.

3.4.3. Surface topography

3.4.3.1. Scanning electron microscopy (SEM)

Scanning electron microscopy (SEM) was used in this research to observe the surface structure and fiber morphology before and after surface modification. The samples were

prepared by mounting 5 mm × 5 mm squares of fabric onto the carbon tape attached to the metal stubs. Then the samples were sputter coated with gold-palladium in a sputter coater for 45 seconds since sputter coating will reduce charging and improve the image of the nonconductive samples. After coating, the samples were placed in the Phenom sample cup and moved into the chamber. Two magnifications were chosen to observe the surfaces. They were 1000X and 5000X. The lower magnification gave a general view of the fabric surface. The higher magnification allowed examination of specific areas along the fiber's surface as well as fiber diameter measurements. Figure 3.12 shows the sputter coater and SEM equipment in the College of Textiles.



(a) (b)
Figure 3.12. (a) Sputter coater; (b) SEM equipment

Meanwhile, the fiber diameters were measured physically from the 5000X SEM images using Image J software. Ten measurements of each sample were taken to calculate the average value.

3.4.4. Mechanical properties

3.4.4.1. Probe bursting strength

Bursting strength test is an easy and effective way to test the mechanical properties and structural integrity of a nonwoven fabric since it provides a strength value that is independent of the fabric direction. This test was included in this research to determine if any of the surface modification treatments changed the mechanical properties and structural integrity of the PLA nonwoven fabric.

The PLA nonwoven specimens were cut into a size of 4cm x 4 cm sized squares and clamped to the platform in the compression cage shown in Figure 3.13. The compression cage was then mounted on an Instron Model 5544 universal mechanical tester. The circular probe had a diameter of 9.5mm and a 100N capacity load cell was used. International standard for Cardiovascular Implants, ISO7198:1998 and standard test method ASTM D3787 was used as reference for this bursting test. The test began as the probe touched the surface of the fabric. The moving speed of the probe was set at 305mm/min. End of the test was set at the point where the fabric lost 50% of its maximum strength. The value of peak load was recorded as the bursting strength of each of the nonwoven specimens. Five specimens were taken for each sample and the average values and standard deviations were calculated. The software used for the test was Blue Hill Version 2.9.



(a)

(b)

Figure 3.13. (a) Instron Model 5544 universal mechanical tester; (b) Compression cage used for probe bursting strength

CHAPTER 4—RESULTS AND DISCUSSIONS

4.1. Fabric thickness measurement

The thickness of the PLA fabric samples treated with different surface modification techniques, and treatment times were recorded before and after surface functionalization. They are presented below.

4.1.1 UVO irradiation

The thickness values with different UVO irradiation times are given in Figure 4.1. The sample with 0min irradiation time was not treated by UVO and served as the control.

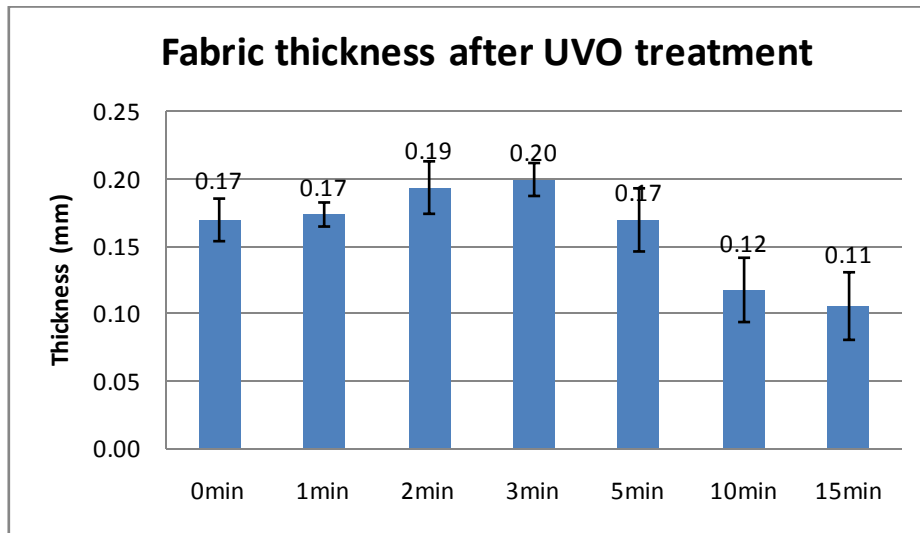


Figure 4.1. Thickness of UVO irradiated PLA samples.

Figure 4.1 shows that as the UVO irradiation time increases, the thickness also has a tendency to increase at first. This is probably due to the reason that the UVO process

promotes the acrylamide to polymerize and graft to the surface of the PLA fabric. However, the fabric thickness begins to fall after three minutes. Thus, it is possible that longer UVO irradiation times are associated with damage to the fiber and fabric structure resulting in a weaker fabric. This will be discussed in the sections on SEM and bursting strength analysis.

4.1.2 Plasma treatment

The thickness values of the PLA fabric samples after exposure to various plasma intensities, gas types and exposure time are given in Figure 4.2.

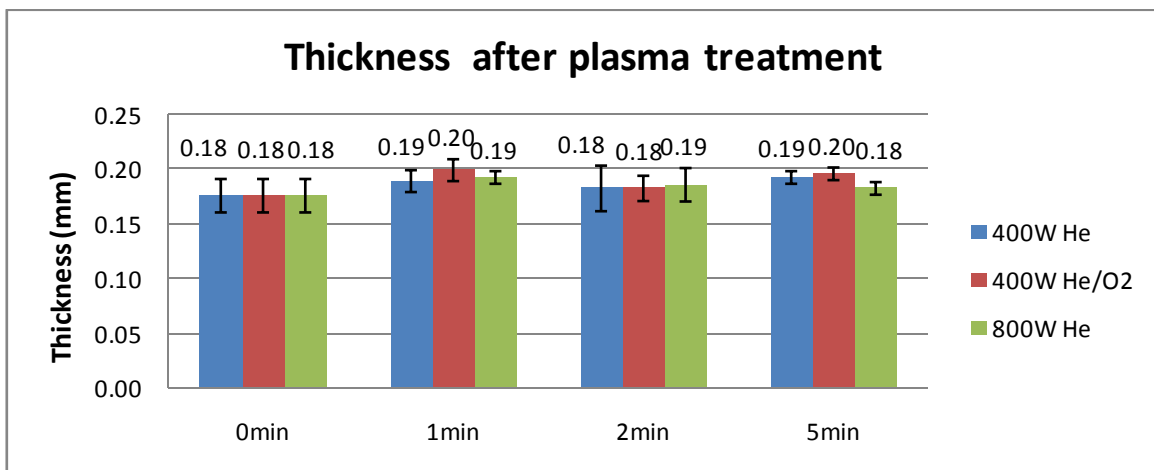


Figure 4.2. Thickness of PLA fabric after plasma treatment with different plasma parameters

From Figure 4.2 it is obvious that the range of thickness values (0.17-0.20mm) is narrow compared to that of the UVO irradiated samples (0.11-0.20mm). Actually the thickness does not change significantly after different durations of plasma irradiation. A possible explanation could be that the plasma treats the sample at the very top of the surface, while UVO penetrates further into the sample. Meanwhile, Figure 4.3 shows how the monomer

concentration affected the fabric thickness. It shows similar results to the previous figure. Thus, from the thickness data it can be concluded that plasma does not change the fabric thickness very much. What can also be inferred is that plasma does not appear to change the physical and mechanical properties of PLA fabric to any significant extent.

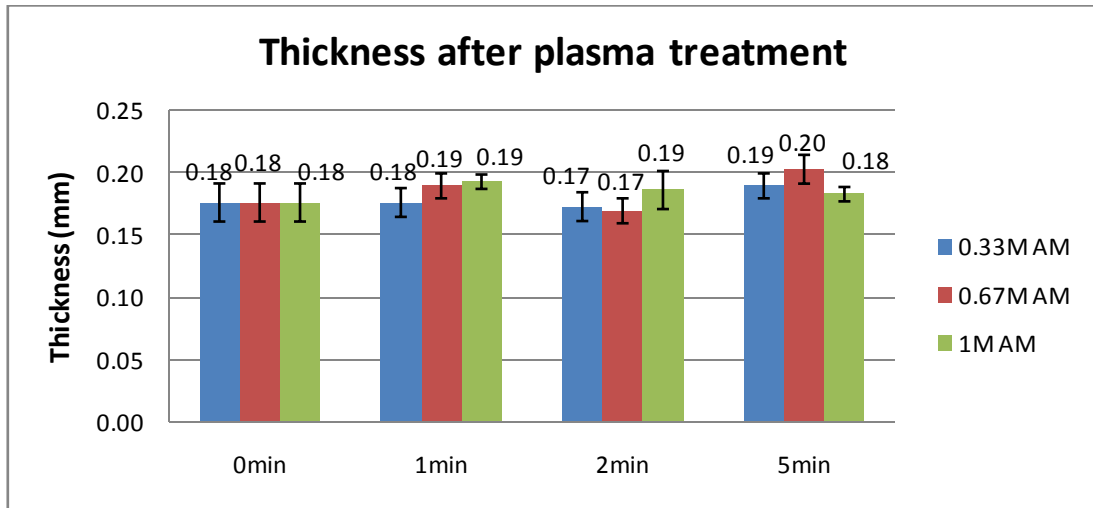


Figure 4.3. Thickness of PLA fabric after plasma treatment with different monomer concentrations

4.1.3 UV irradiation

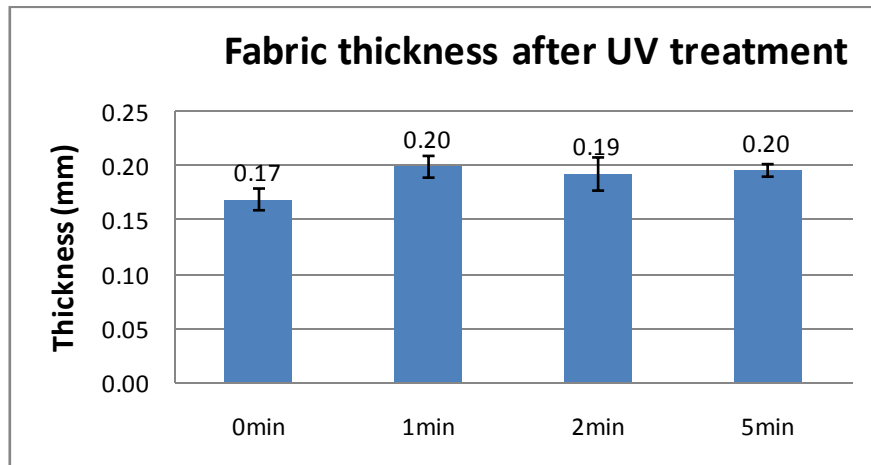


Figure 4.4. Thickness of PLA fabric after UV irradiation

The thickness values after different UV irradiation times are given in Figure 4.4. From the data it is observed that UV irradiation does not cause a significant change in fabric thickness. Compared to the control group which was not irradiated by UV light, the fabric thickness has increased by a marginal amount which is probably due to the swelling of the fibers in solution and the polymerization process.

4.2. Surface functionalization

This part discusses the results of the acrylamide monomer being polymerized and grafted onto the surface of the PLA nonwoven fabric. The three different methods, namely UVO, UV and plasma are discussed one at a time. Different surface analytical techniques, such as FTIR, contact angle measurements and XPS have been carried out to compare the effectiveness of the different treatments. In addition, SEM images were taken to observe changes in the surface morphology of the PLA fibers.

4.2.1. UVO polymerization

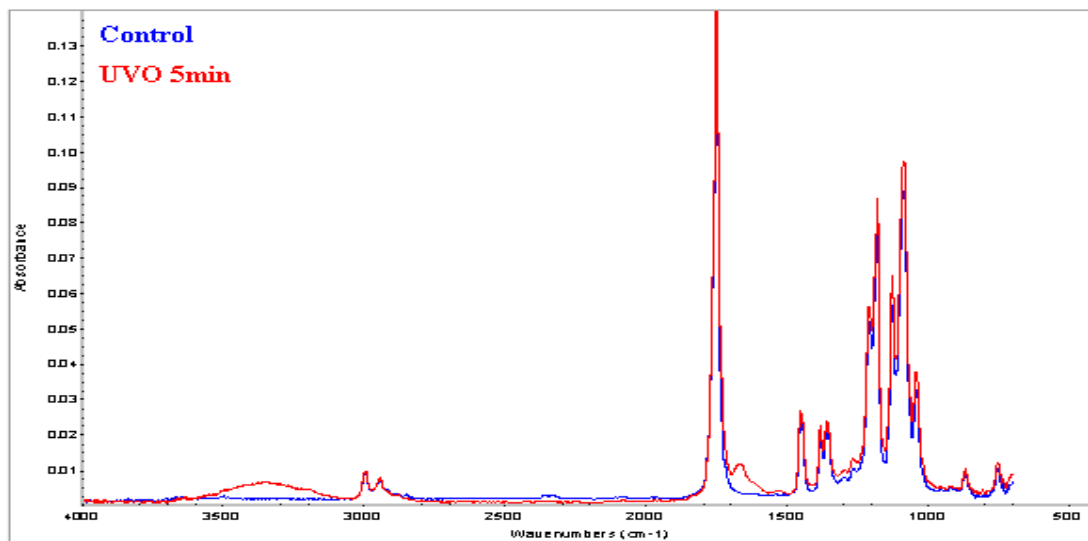


Figure 4.5. FTIR spectra of the original control PLA sample (in blue) and the PLA sample after exposure to UVO for 10min (in red)

In Figure 4.5, the blue spectrum is the PLA control sample without any treatment and it shows some typical PLA peaks. The band originated from C=O stretching vibrations is situated at 1745cm^{-1} . There are three bands in the $1300\text{-}1500\text{cm}^{-1}$ range that are attributed to symmetric and asymmetric deformation vibrations of the C-H bonds in the methyl groups. And the bands appearing in the range of $1000\text{-}1300\text{cm}^{-1}$ are most likely the vibrations of C-O in the PLA polymer chain.

In comparison, the spectrum for the PLA sample exposed to UVO shows some significant differences which suggest that some chemical modification did take place on the surface. One additional peak is observed in the $3200\text{-}3500\text{cm}^{-1}$ range, which is probably the N-H group vibration in polyacrylamide. Another small peak appears between $1650\text{-}1750\text{cm}^{-1}$

which is the vibration associated with C=O in polyacrylamide. These peaks confirm that polyacrylamide has been attached to the surface of PLA fabric.

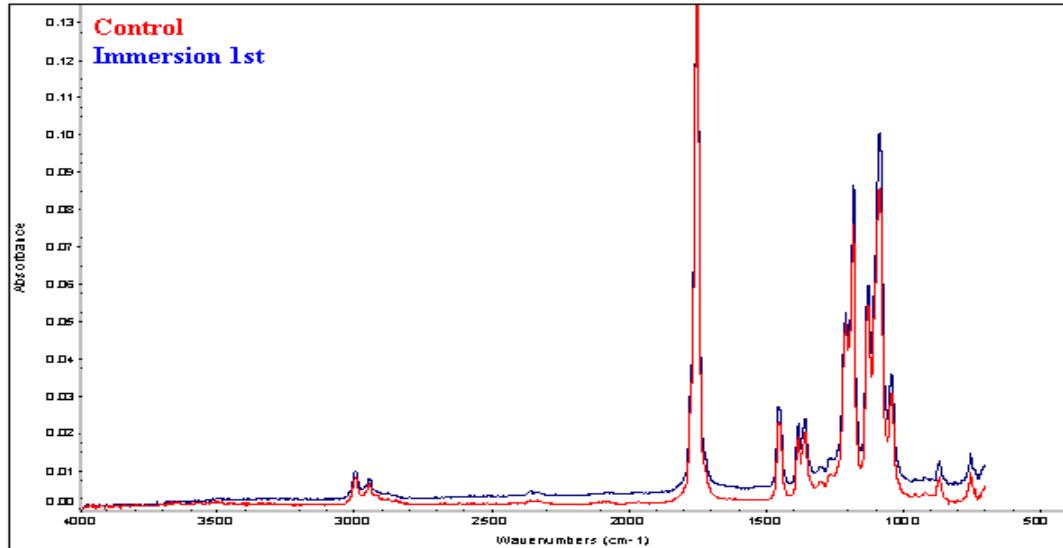


Figure 4.6. FTIR spectra of the original control PLA (in red) and the PLA sample after immersion in acrylamide but without UVO (in blue)

In order to determine if UVO was required to polymerize the acrylamide on the surface of the PLA, the following two samples were compared. One was the original PLA control sample and the other was the PLA fabric immersed in acrylamide solution for 2 hours but without any UVO irradiation. Both samples were analyzed by FTIR. From Figure 4.6, it can be seen that there's no significant difference between the two spectra, which confirms that UVO plays an important role in attaching polyacrylamide to the surface of PLA fabric.

4.2.1.1. Experimental variables

The experimental sequence, irradiation time and monomer concentration were included as three experimental variables in this study in order to determine the optimal conditions for acrylamide polymerization.

4.2.1.1.1. Sequence variable

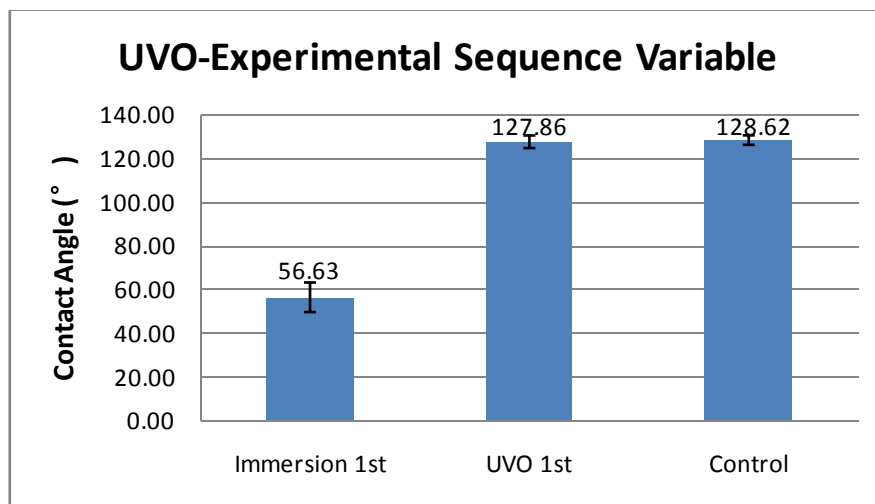


Figure 4.7. Effect of experimental sequence on contact angle

Figure 4.7 shows the value for contact angle depending of the experimental sequence used. It can be seen that the original PLA control fabric is a hydrophobic material with contact angle of 128.62 ± 2.17 degrees. The sample that was immersed in acrylamide first and then UVO irradiated for 5min has an average contact angle value of 56.63 degrees which shows a significant decrease compared to the original PLA. This suggests that UVO irradiation was responsible for generating reactive species which resulted in polyacrylamide grafting onto

the PLA surface. The N-H groups in polyacrylamide are hydrophilic and when they attach to the surface of the hydrophobic PLA, the contact angle decreases sharply. However, the sample that was UVO irradiated first and then immersed in acrylamide does not show a significant decrease in contact angle. Its average contact angle is equivalent to that of the original PLA control. This indicates that with this sequence the UVO irradiation was not responsible for a decrease in contact angle, nor was the polyacrylamide grafted to the PLA surface when it was in solution.

4.2.1.1.2. Irradiation time variable

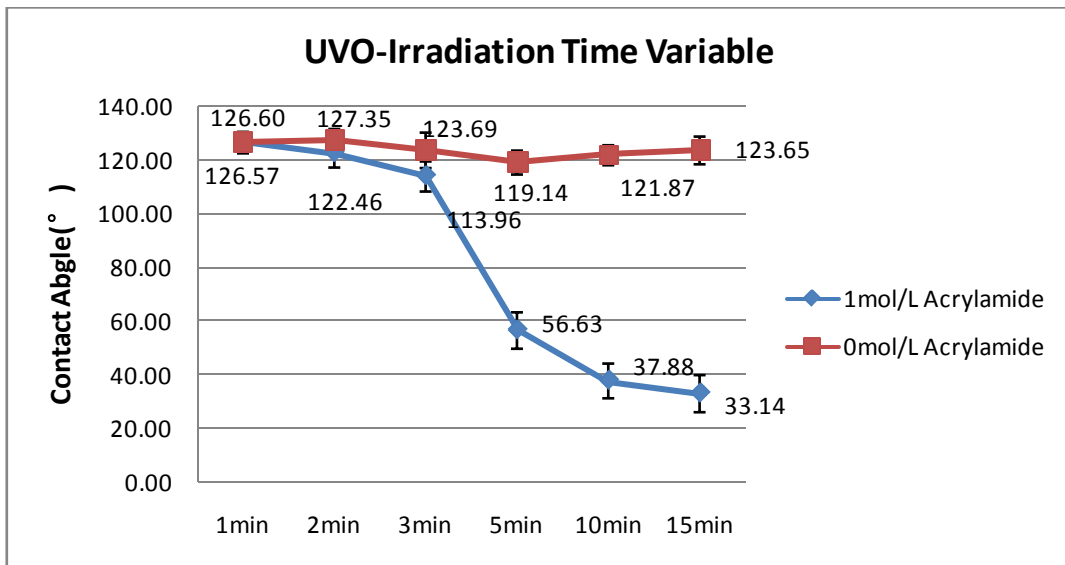


Figure 4.8 Effect of irradiation time on contact angle

The red (upper) line in Figure 4.8 shows the contact angle value for the control PLA without acrylamide immersion. It shows that the UVO irradiation alone was not the major cause for

surface modification and a decrease in contact angle. The blue (lower) line shows that the average contact angle did fall as the UVO irradiation times increased. With at least 5 min of irradiation, the contact angle fell below 60 degrees which is in the hydrophilic range. This supports the hypothesis that longer irradiation times generate more free radicals on the surface of the PLA fabric which results in a greater amount of grafting.

4.2.1.1.3. Monomer concentration variable

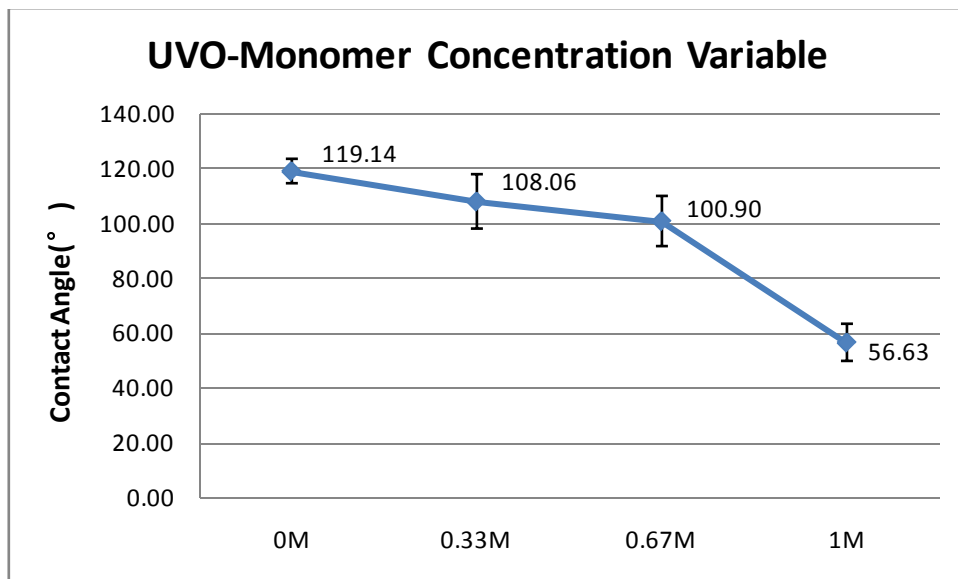


Figure 4.9. Effect of monomer concentration on contact angle

Figure 4.9 shows that using a fixed 5 min irradiation time the contact angle decreased as the monomer concentration increased from 0M to 1M. This result suggests that the presence of a higher quantity of monomer in solution created more reactive sites and allowed more polymerization and grafting to occur. This resulted in a more hydrophilic surface. It should

be noted that the zero monomer concentration corresponds to exposing the samples to UVO irradiation without any monomer immersion.

Below is Figure 4.10, which shows the surface-droplet interaction during the contact angle measurements. The substrate in (a) is the control PLA which is clearly hydrophobic, while (b) has polyacrylamide grafted to PLA surface and is clearly hydrophilic. |

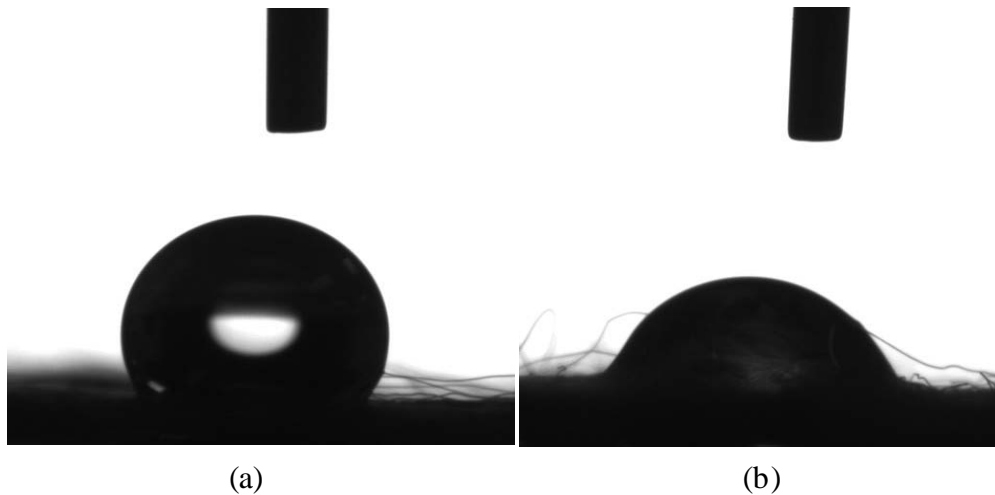


Figure 4.10. Surface-droplet interaction during contact angle measurement (a). Control PLA; (b). polyacrylamide grafted PLA

4.2.2. Plasma polymerization

Compared to the original PLA, the FTIR spectrum of the PLA sample exposed to plasma for 5min under 800W in helium shows some differences which suggest that some chemical modifications took place at the PLA surface under these conditions (Figure 4.11). A small additional peak is observed in the $3200\text{-}3500\text{cm}^{-1}$ range, which is probably due to the N-H group in polyacrylamide. Another small peak appears in the $1650\text{-}1750\text{cm}^{-1}$ range which is

associated with C=O vibration in polyacrylamide. These peaks are similar to those found in the UVO irradiated samples, which indicates that polyacrylamide has also been grafted onto the PLA fabric surface using plasma treatment. However, one interesting phenomenon is that the peaks in the plasma treated samples are not so high as those irradiated by UVO. This might be due to the difference in the depth of surface penetration of the UVO and plasma. It appears that with the same monomer concentration and irradiation time, the UVO treatment causes a deeper penetration and more extensive modification than the plasma treatment which takes place only at the very top surface. This can be monitored by the different surface analysis techniques, and correspond to the fact that ATR-FTIR has a deeper penetrating depth of 0.5-2 micrometers compared to XPS with its penetration depth of 1-10nm and TOF-SIMS with only 1-2nm. The XPS and TOF-SIMS results in the following section show that there was a considerable amount of nitrogen on the surface of the treated PLA samples.

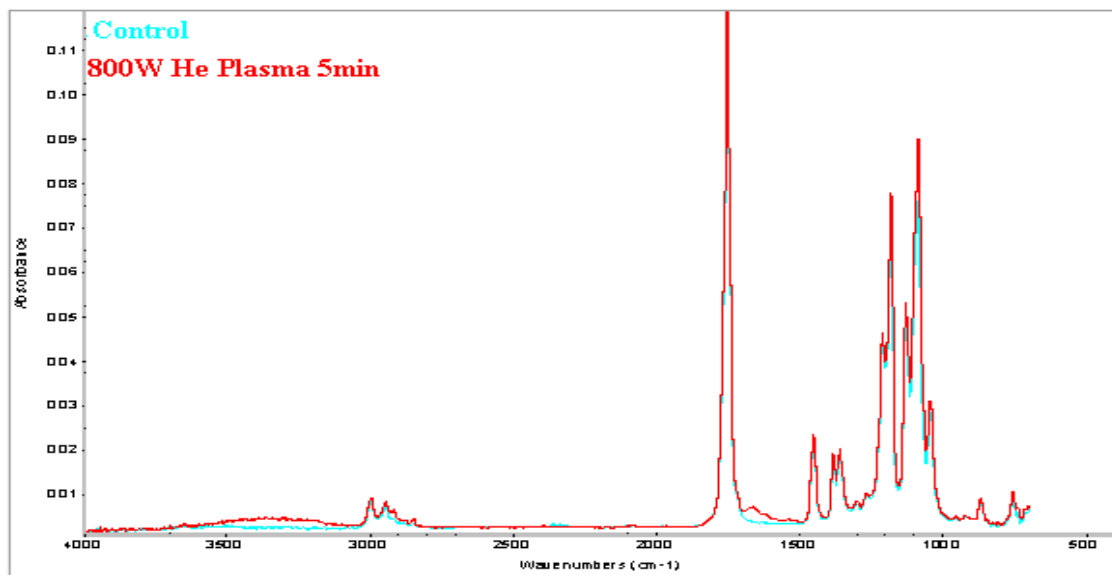


Figure 4.11. FTIR spectra of original PLA control (in blue) and PLA after 5 minutes of 800W helium plasma treatment (in red)

4.2.2.1. Experimental variables

The plasma intensity, irradiation time, gas type and monomer concentration were four variables that were included in the study to determine the optimal conditions for acrylamide polymerization on PLA fabric.

4.2.2.1.1 Plasma intensity

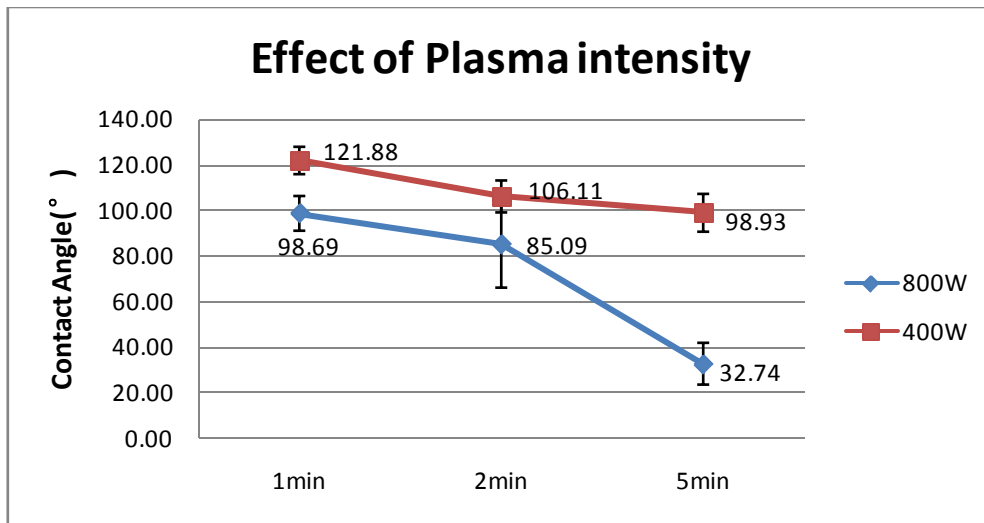


Figure 4.12. Effect of plasma intensity on contact angle

Figure 4.12 shows how plasma intensity affected the contact angle of the treated PLA samples. The red (upper) line shows the results for the 400W and the blue (lower) one represents the 800W plasma intensity. From the graph it is easy to observe that the PLA treated with 800W had a lower average contact angle than the PLA treated with only the 400W plasma. This corresponds to the hypothesis that a higher plasma intensity generates more free radicals on the surface of the PLA which enables a greater amount of grafting to the PLA surface. For the PLA sample exposed to 800W for 5min, the contact angle fell to

below 40 degrees which is hydrophilic. This suggests that the higher intensity plasma was able to modify the surface of the PLA by a considerable and significant amount.

4.2.2.1.2 Irradiation time

Figure 4.13 shows how the average contact angle changed when exposed to increasing durations of 800W helium plasma. It is obvious that the contact angle decreased with increasing of irradiation time. When treated for 5 min, the contact angle decreased from 128 degrees for original PLA control to only 33 degrees. This again suggests that with the increase in plasma exposure, more free radicals are generated, which enables a greater amount of grafting on the PLA surface. For other plasma exposure conditions, a decrease in contact angle with increased plasma exposure was also observed.

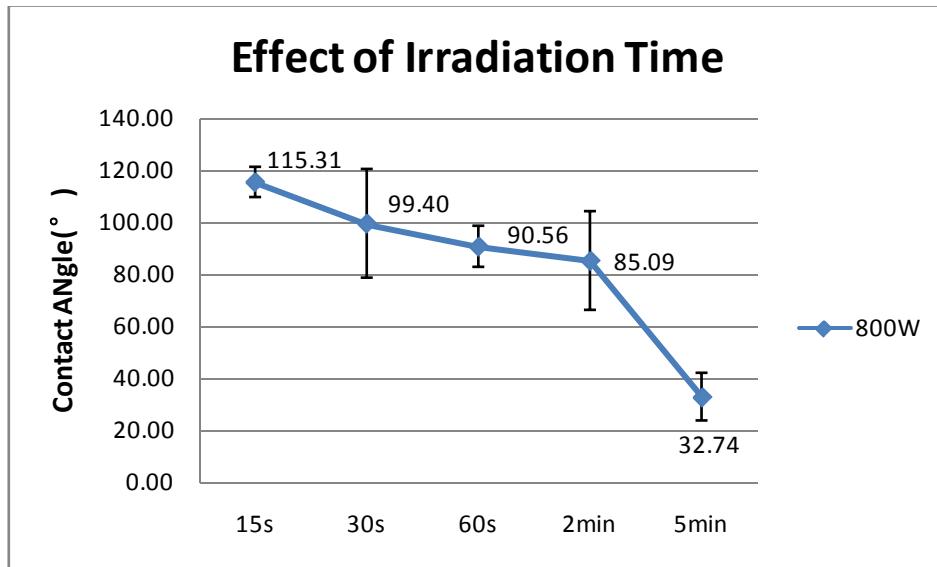


Figure 4.13. Effect of irradiation time on contact angle value

4.2.2.1.3 Gas type

Figure 4.14 shows the resulting changes in contact angle when different types of gas were used to create the plasma. A plasma intensity of only 400W was used since higher intensity plasma could not be achieved when 0.5% oxygen was added. Figure 4.14 shows that the average contact angle after treatments of helium alone is lower than that for the helium and oxygen mixture. The interaction between the plasma and the PLA surface is complicated by the fact that the plasma involves many different species, such as electrons, photons, ions and neutrals. So the chemical changes which take place on the PLA surface are closely related to the type of gas in the plasma. When a small amount of oxygen is added to the helium atmosphere, there is a substantial increase in breakdown voltage, which is likely to reduce the plasma density and compromise the effectiveness of the plasma. As a result, fewer free radicals are generated and the extent of grafting of polyacrylamide onto the PLA surface decreases as well. This explains why the PLA contact angle for oxygen containing plasma remains higher than that for pure helium plasma.

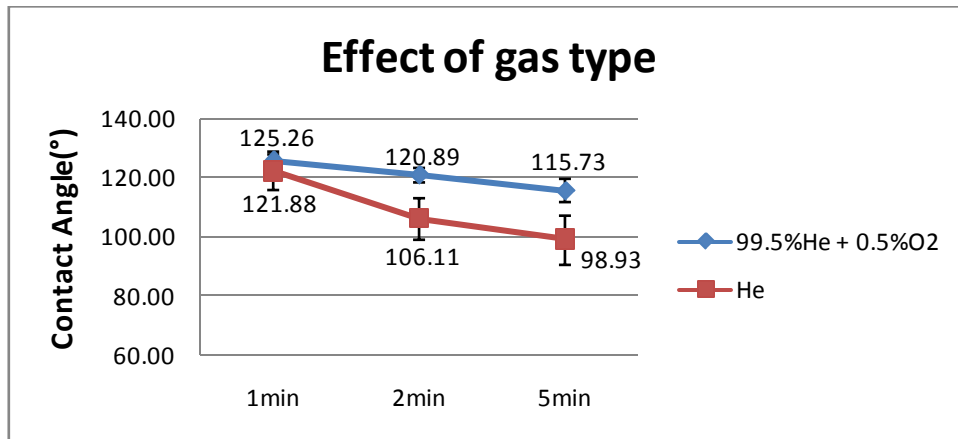


Figure 4.14. Effect of gas type on contact angle value

4.2.2.1.4 Monomer concentration

Figure 4.15 shows the changes in contact angle and surface wetting characteristics with increasing monomer concentration. As the monomer concentration increased from 0.33M to 1M at intervals of 0.33M, the contact angle decreased. In addition, with increasing plasma exposure times, particularly at higher monomer concentrations, the contact angle fell significantly to hydrophilic levels. This may be due to the fact that higher monomer concentrations facilitate a higher grafting percentage, because the more frequent molecular collisions between the species can increase the rate of polymerization. The decrease in contact angle is mainly due to the presence of N-H group in acrylamide being attached to the PLA surface.

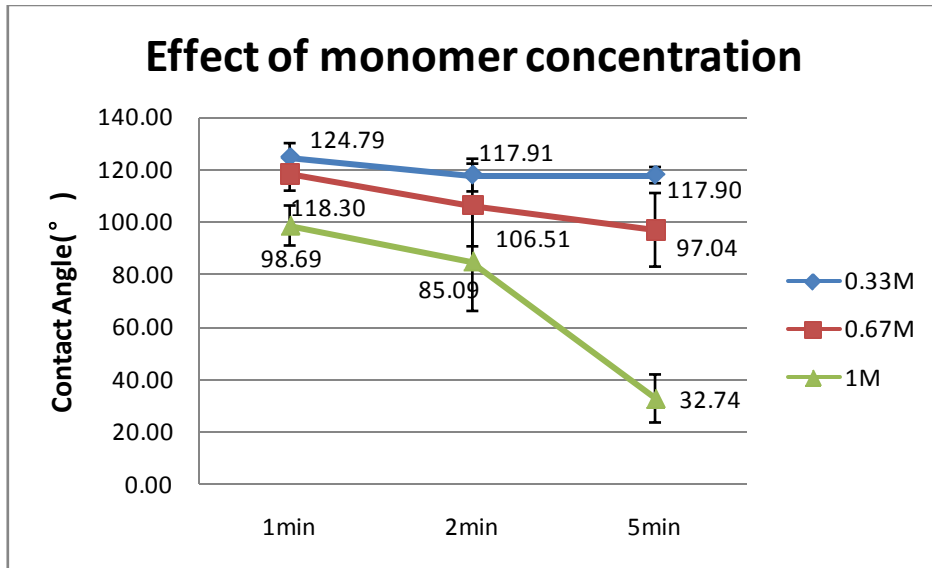


Figure 4.15. Effect of monomer concentration on contact angle

4.2.3 UV polymerization

Figure 4.16 shows the FTIR spectra of the original PLA control and the PLA fabric after 5 minutes of UV irradiation. Actually there is no significant difference between these two spectra. There are two possible reasons that could explain this. The first reason is that the comparatively short duration of UV irradiation does not result in significant surface modification to the PLA. The second reason could be that the higher penetration depth of the FTIR signal is not sensitive enough to monitor changes that only occur at the very top surface layer.

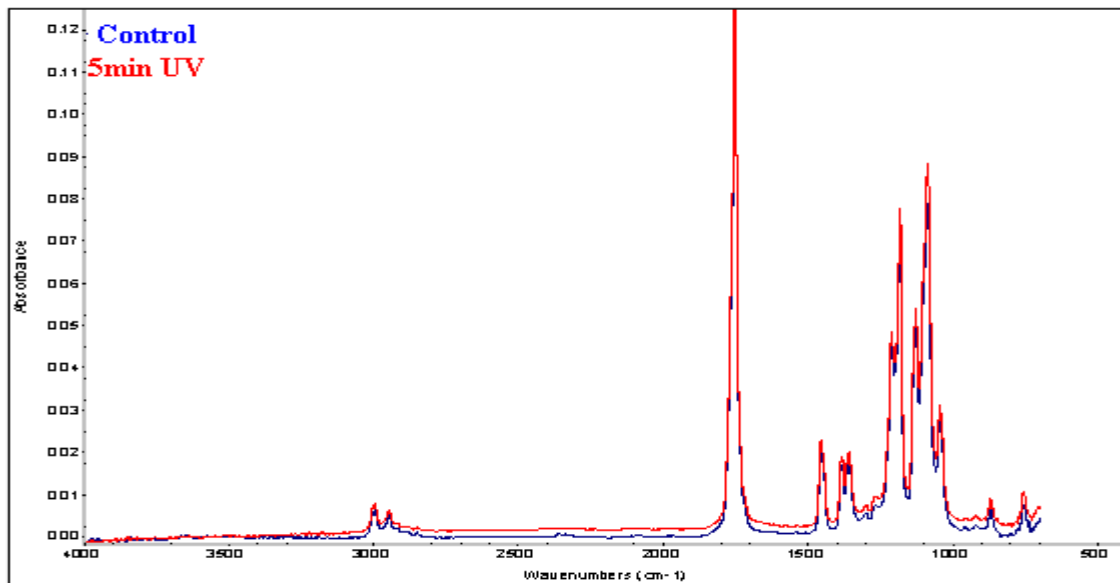


Figure 4.16. FTIR spectra of original PLA control (in blue) and PLA after 5 minutes of UV irradiation (in red)

Below is Figure 4.17 showing changes in contact angle under different UV irradiation times. The original PLA control had an average contact angle of 128.62 degrees. From the figure it

can be seen that short UV irradiation times of 1 min do not change the contact angle significantly. At longer UV irradiation times, there was a decreasing trend in contact angle. However, it was only mild compared to the UVO and plasma irradiated samples.

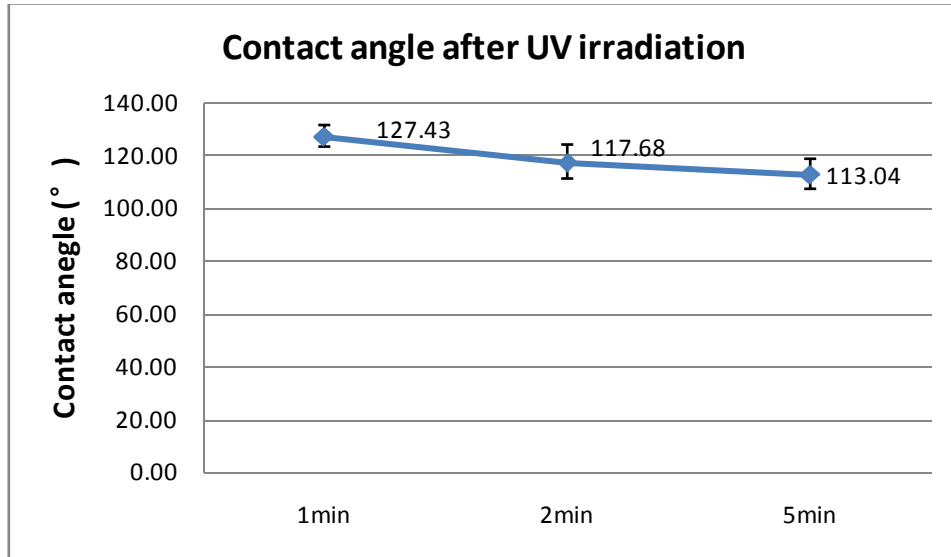


Figure 4.17. Effect of UV irradiation time on contact angle

4.3. Genipin attachment and collagen immobilization

After surface functionalization, genipin and collagen were attached to the surface of the activated PLA fabric. Various test methods were used to detect the presence of genipin and collagen.

4.3.1. Fourier transform infrared (FTIR) spectroscopy

Figure 4.18 shows the spectra of the original PLA control, the PLA after polyacrylamide activation, after genipin attachment and collagen immobilization. For these samples, UVO

was used as the surface functionalization method. Each PLA sample served as the precursor for the next treatment. As discussed in the previous sections, there were two additional peaks added to the original PLA spectrum. One was observed in the $3200\text{-}3500\text{cm}^{-1}$ range which is probably due to the N-H group vibration in polyacrylamide. Another small peak appeared in the $1650\text{-}1750\text{cm}^{-1}$ range which is caused by the C=O group in polyacrylamide. These peaks confirm that polyacrylamide has been polymerized in situ and is attached to the PLA substrate.

As for the genipin spectrum, there were no major differences compared with the previous spectrum, except that the peaks in the range of $3200\text{-}3500\text{cm}^{-1}$ and $1650\text{-}1750\text{cm}^{-1}$ had virtually disappeared. That is probably because the genipin was now attached to the polyacrylamide which eliminated these characteristic peaks.

When collagen was immobilized, the spectrum then showed peaks between $3100\text{-}3500\text{cm}^{-1}$ which probably belonged to the N-H vibration in amide groups and O-H in the carboxylic acid groups of collagen. Meanwhile, the peak between 1600 and 1700cm^{-1} indicates that there was a C=O vibration in the structure which was likely to belong to the amide and carboxylic acid groups. These peaks confirm the presence of collagen on the PLA activated surface.

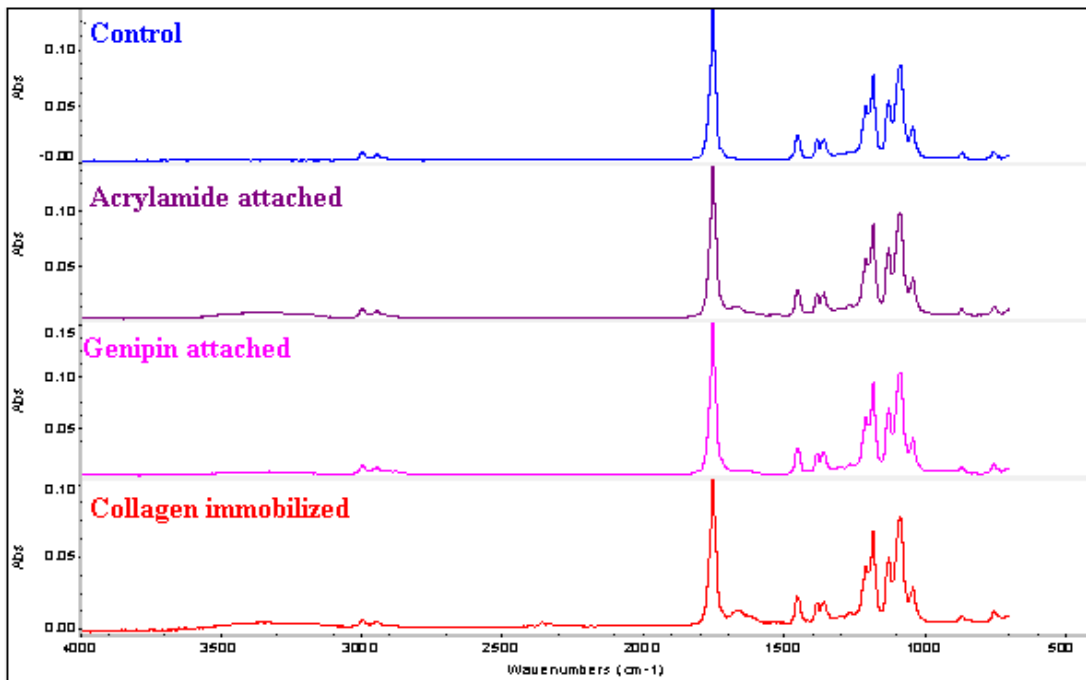


Figure 4.18. FTIR spectra of PLA under four different surface modification conditions

4.3.2. Contact angle

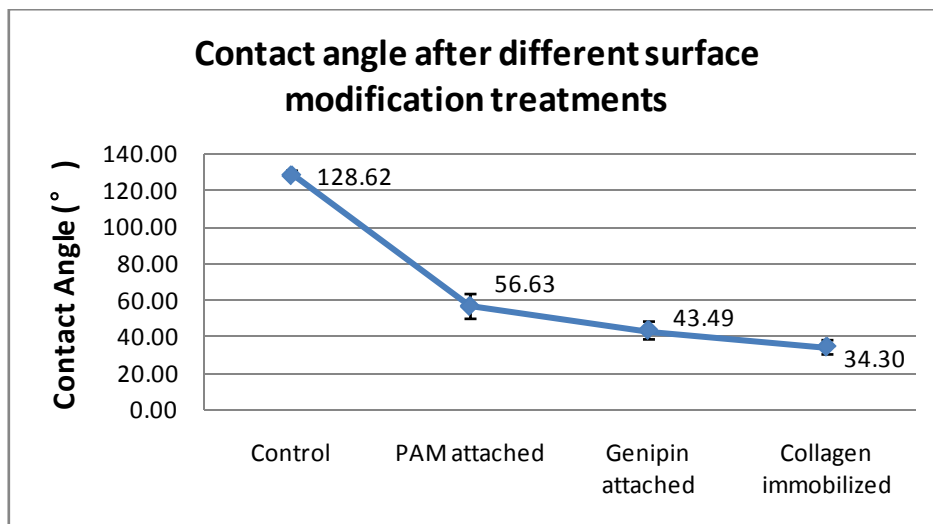


Figure 4.19. Contact angle after four different surface modification treatments

Figure 4.19 shows the average contact angle of the original PLA control, the PLA following polyacrylamide activation, after genipin attachment and collagen immobilization PLA. The original PLA had an average contact angle of 128 degrees which is hydrophobic. When polyacrylamide was polymerized on the surface, the contact angle fell to 56 degrees. This is probably due to the addition of amino groups to the surface which improves the surface hydrophilicity.

When genipin was attached, the contact angle value dropped an additional 12 degrees. This suggests that genipin with its hydroxyl groups had been immobilized onto the surface and these hydrophilic groups contributed to the decrease in contact angle.

After collagen immobilization, the contact angle dropped further to 34 degrees. This confirms the presence of collagen on the PLA surface. The carboxylic acid and amide groups in collagen play an important role in reducing the contact angle and improving the biocompatibility of the PLA fabric.

4.3.3. X-ray Photoelectron Spectroscopy (XPS)

The XPS technique is used as a quantitative method for elemental analysis. The PLA control, the acrylamide activated PLA, the genipin treated PLA as well as the collagen immobilized PLA were all tested by XPS and the elemental compositions are listed below in Table 4.1. PLA is composed of C, H, O only, without N. It could be seen that after surface functionalization, the percentage of nitrogen increased from 0% to 3.73% which suggests that acrylamide had been grafted onto the surface of the PLA fabric. After the genipin treatment,

the nitrogen content decreased to 2.9% probably because genipin had been added to the surface of the acrylamide and it contains no nitrogen. However, when collagen was immobilized on the surface, the nitrogen content increased again to 4.63%, which confirms that nitrogen containing collagen had been successfully immobilized.

Table 4.1. Elemental composition of PLA before and after each treatment

	C(%)	O(%)	N(%)	O/C
Control PLA	61.22	38.78	-	0.63
Acrylamide attached PLA	59.97	36.30	3.73	0.61
Genipin treated PLA	60.55	36.55	2.90	0.60
Collagen immobilized PLA	57.54	37.83	4.63	0.66

Figure 4.20 shows the full XPS spectrum of control PLA. Only C and O are detected. The C_{1s} spectrum of the original PLA shows major peaks with binding energies of 284.9 eV, 287.0eV, 288.9 eV corresponding to C-H, C-O and C=O respectively as shown in Figure 4.21.

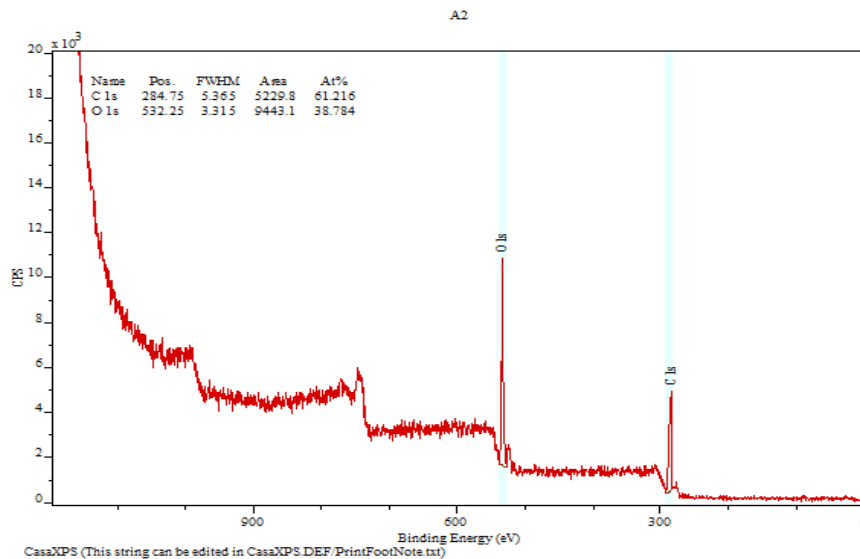


Figure 4.20. Full spectrum of control PLA

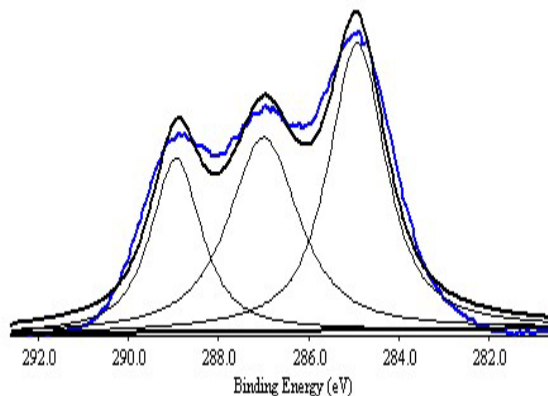


Figure 4.21. Deconvoluted C1s spectrum of control PLA

After treatment with acrylamide and UVO, a nitrogen peak appears in the spectrum as shown in Figure 4.22 and has a percentage of 3.73%. The deconvoluted N1s spectrum of acrylamide attached to PLA in Figure 4.23 shows a major peak with binding energy of 399.4eV corresponding to the N-H group. This evidence indicates that acrylamide had been successfully polymerized and attached to the PLA surface.

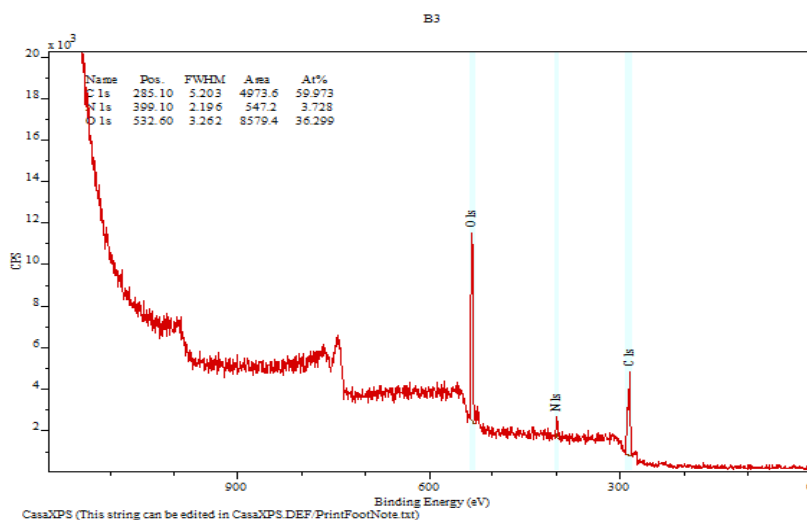


Figure 4.22. Full spectrum of acrylamide attached to PLA

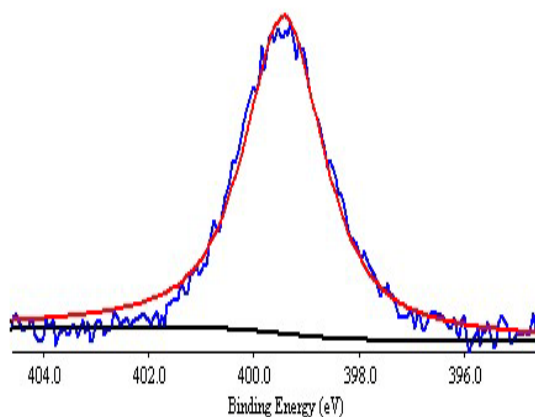


Figure 4.23. Deconvoluted N1s spectrum of acrylamide attached to PLA

4.3.4. Time-of-flight mass spectrometry (TOF-SIMS)

TOF-SIMS is a surface sensitive technique with a penetration depth of 1-2nm. Thus it is able to detect the chemistry of the very top surface. Meanwhile, this technique can also monitor and present the distribution and uniformity of collagen immobilized on the PLA surface.

The TOF-SIMS spectra are presented in a plot of intensity versus mass. Although there are a large number of peaks shown in the positive and negative ion spectra, only characteristic peaks are discussed here. Figure 4.24 and Figure 4.25 present the positive and negative spectra of the control PLA (Sample1), the acrylamide functionalized PLA (Sample2), the genipin attached PLA (Sample3) and the collagen immobilized PLA (Sample4), respectively.

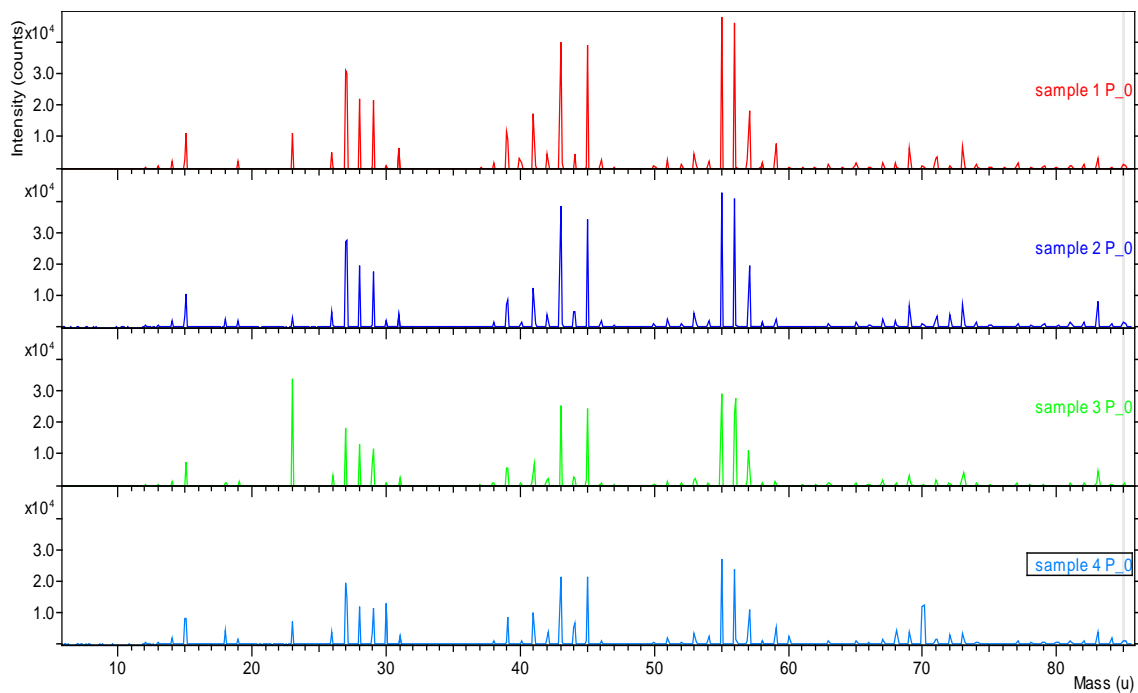


Figure 4.24. Positive spectra of four PLA samples

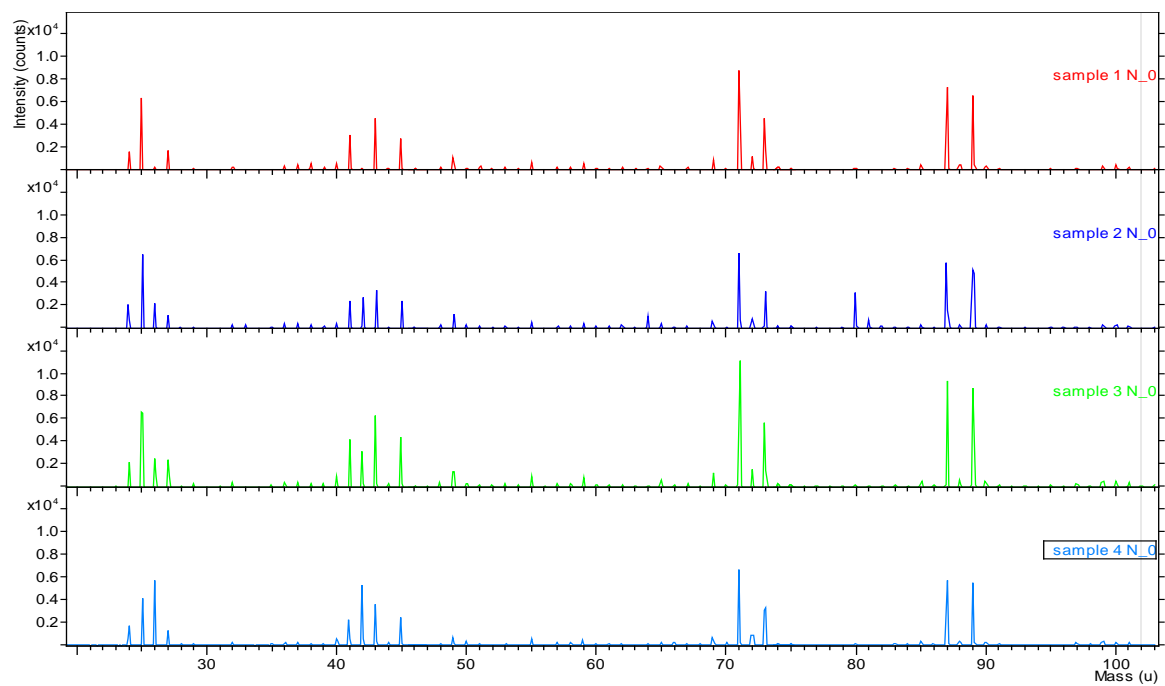


Figure 4.25. Negative spectra of four PLA samples

Each peak represents a secondary ion at a certain mass (u). Untreated PLA consists of C, N, O atoms and there are several characteristic peaks for PLA which can be found in the red spectrum (Sample1). They are positive ions such as $C_2H_3O^+$ at 43u, $C_2H_5O^+$ at 45u, $C_3H_3O^+$ at 55u, $C_3H_7O^+$ at 59u and negative ions such as $C_3H_3O_2^-$ at 71u, $C_3H_3O_3^-$ at 87u and $C_3H_5O_3^-$ at 89u. Note that the 56u peak is the highest and most intense, so it can be used as the dominant peak for the presence of PLA. The negative spectrum of PLA exhibits fewer and weaker peaks compared to the positive spectrum, so it is less important when attempting to identify PLA.

When acrylamide is attached to the PLA surface (Sample2), some changes on the spectrum are observed such as NH_4^+ at 18u, CN^- at 26u, CNO^- at 42u. These peaks indicate that nitrogen was detected on the surface of PLA after surface functionalization. This confirms that acrylamide was attached to the surface of PLA fabric.

After genipin attachment, there are not so many new peaks generated (Sample3). This was probably because genipin has a similar chemical composition and ionization behavior to PLA which makes it difficult to detect when combined with PLA spectra. However, it is notable that some characteristic peaks of PLA show a significant reduction in height, such as $C_2H_3O^+$ at 43u, $C_2H_5O^+$ at 45u, $C_3H_3O^+$ at 55u and $C_3H_7O^+$ at 59u. These observations indicate that some surface modification took place and genipin was been attached to PLA fabric surface.

The last step was collagen immobilization. Following the treatment, many characteristic peaks for collagen were found in the spectra (Sample4). New peaks were observed including

CH_2NH_2^+ at 30 u and $\text{C}_4\text{H}_8\text{N}^+$ at 70u in the positive spectrum as well as CN^- at 26 u and CNO^- at 42 u in the negative spectrum as shown in Figure 4.24 and Figure 4.25, respectively. These characteristic peaks confirm the presence of collagen immobilized on the surface of the PLA fabric since such peaks did not appear in any of the previous samples. Meanwhile, the characteristic peaks for PLA in Sample4 are not so high and intense as those in the control spectrum. This observation supports the fact that collagen was successfully immobilized on the PLA surface.

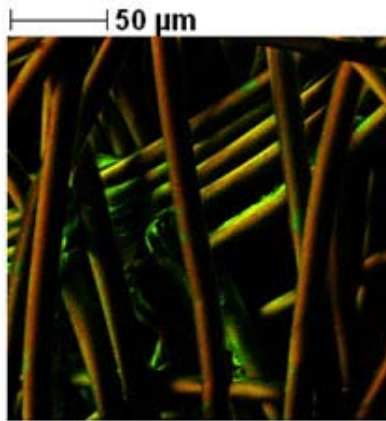


Figure 4.26. Chemical mapping images showing overlay of the collagen positive ion image in green over the PLA $\text{C}_3\text{H}_3\text{O}^+$ ion image in red

To further study the uniformity of the immobilized collagen on the PLA surface, chemical mapping was conducted. The overlaid images in Figure 4.26 show the collagen NH_4^+ , CH_2NH_2^+ , $\text{C}_4\text{H}_8\text{N}^+$ ion image in green plus the PLA $\text{C}_3\text{H}_3\text{O}^+$ ion image in red. It can be seen that some areas are covered with a green image while other places are mainly red. This confirms that collagen was immobilized on the PLA surface, but the uniformity of the coating was not very even and needs to be improved.

4.4. Surface Morphology and Fiber Diameter

In this section, different steps in the surface modification process of PLA are shown in terms of their SEM images from Figure 4.27 to Figure 4.32 in order to observe the morphological changes at the fiber surface. Two magnifications were used: 1000 \times and 5000 \times . The images of UVO and plasma treated PLA are compared. Meanwhile, fiber diameters are measured for the four PLA samples and the results are listed in Figure 4.33.

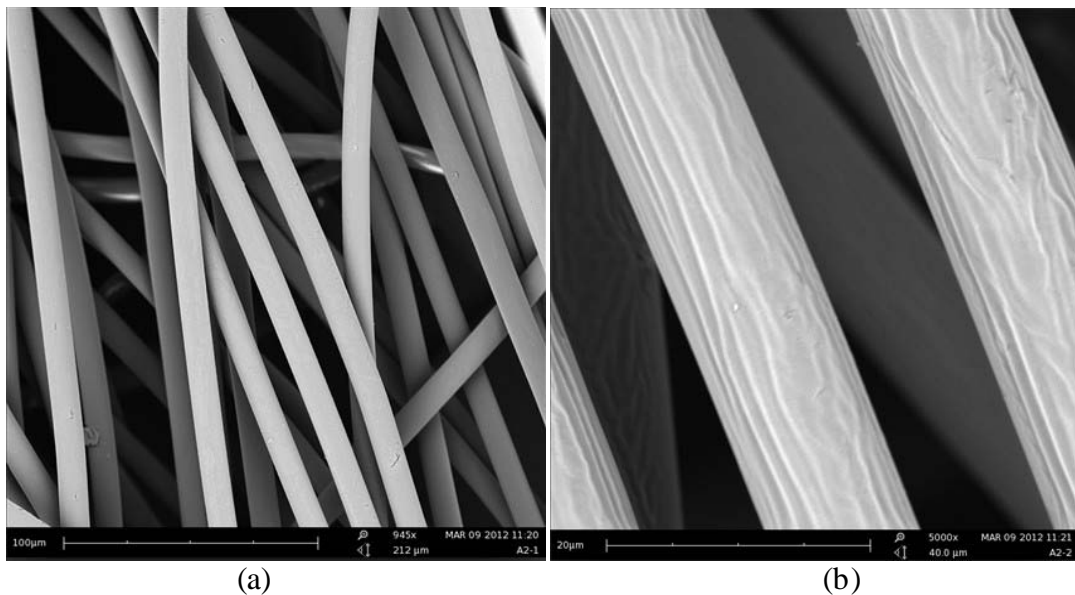


Figure 4.27. SEM image of the original PLA control at 1000X (a) and 5000X (b)

Figure 4.27 shows the original untreated PLA. The fibers are clean and smooth. As shown at 1000X, it can be seen that the thickness of fibers are relatively uniform with an average diameter of 10.65mm.

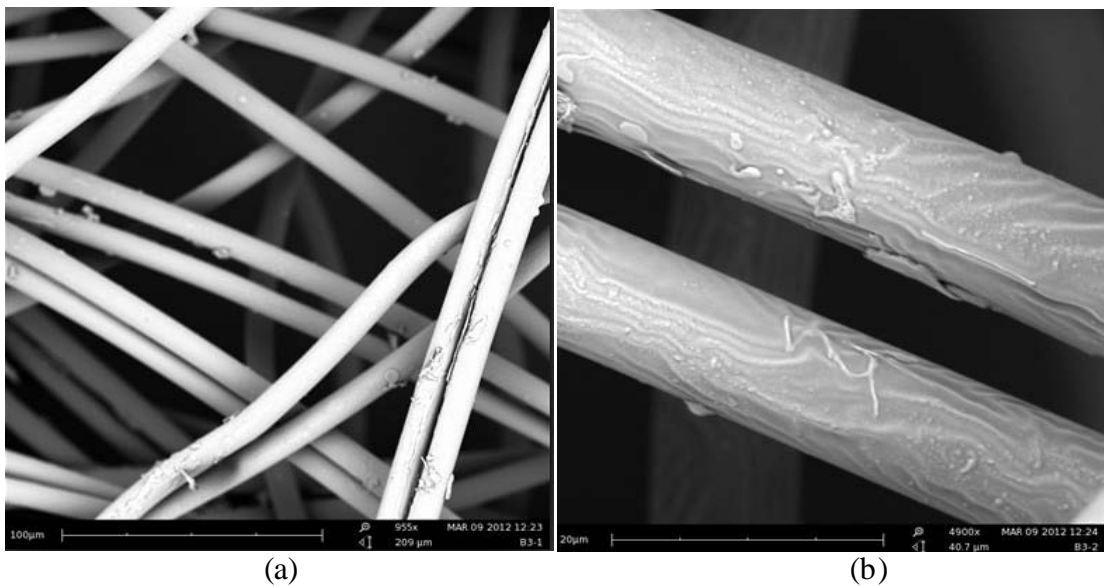


Figure 4.28. SEM image of PLA after 1 min of UVO irradiation at 1000X (a) and 5000X (b)

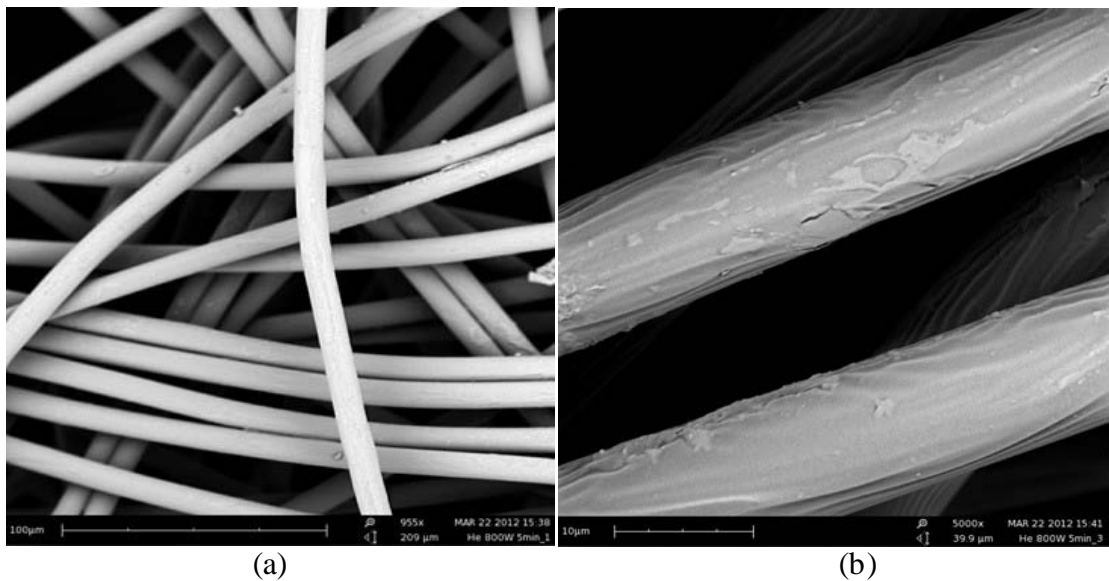


Figure 4.29. SEM image of PLA after 1 min of plasma exposure at 1000X (a) and 5000X (b)

When irradiated by UVO or plasma for 1 min as shown in Figure 4.28 and Figure 4.29, some changes are observed on the surface of the fibers. There is some deposition over the fiber

surface suggesting that the acrylamide was attached. However, it appears that the deposition of acrylamide is not very uniform along the fiber surface.

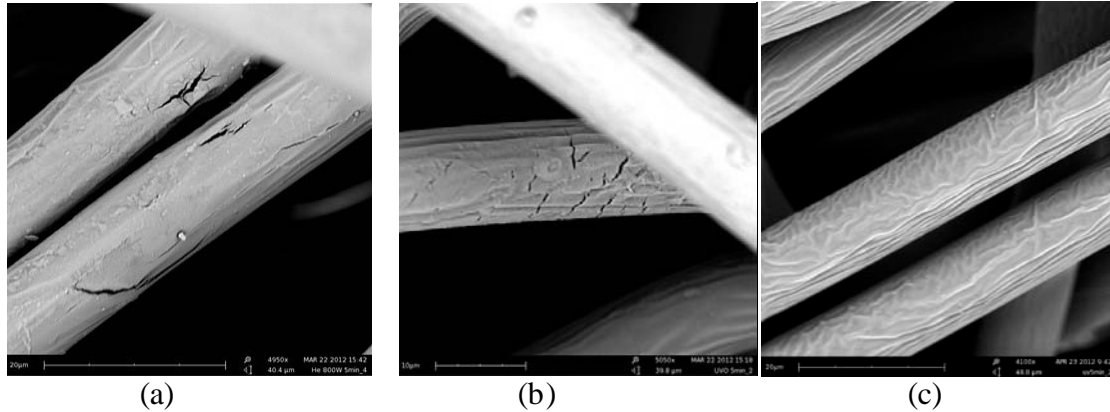


Figure 4.30. SEM image of PLA after 5 min of UVO irradiation (a), plasma exposure (b) and UV irradiation (c) at 5000X

Figure 4.30 presents SEM images of the PLA treated fibers showing their surface morphology after longer periods of UVO, plasma and UV exposure. It can be seen that there are visible cracks on the PLA surface for the UVO and plasma treated samples. However, the cracks on the UVO irradiated sample are more frequent and severe compared to those following plasma treatment. This corresponds to the results from the bursting test. These observations indicate that UVO irradiation is more intense and damaging than either of the plasma or UV treatment.

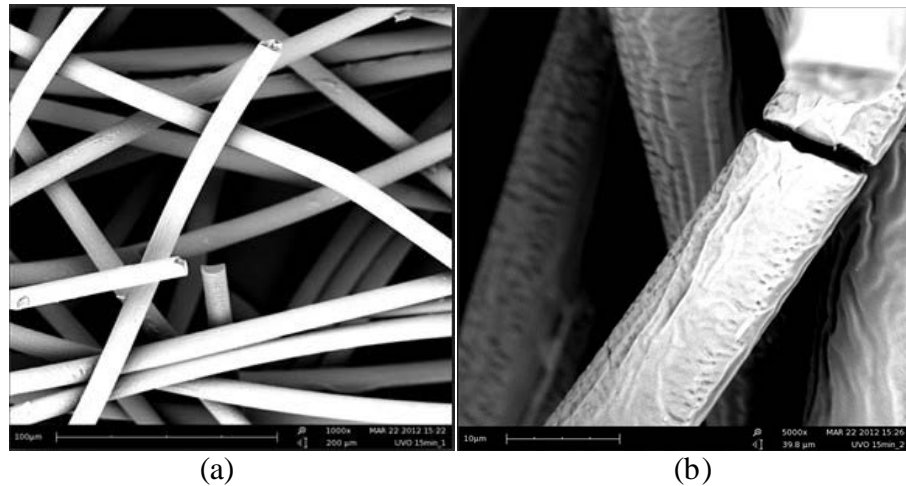


Figure 4.31. SEM image of PLA after 15 min of UVO irradiation at 1000X (a) and 5000X (b)

The fibers irradiated by UVO for 15 min appear to be severely damaged. Many fibers are broken as shown in Figure 4.31. The 5000X image shows clearly the broken end of a fiber and the rough surface. These observations explain the significant decrease in bursting strength that was observed following UVO exposure (see Section 4.5).

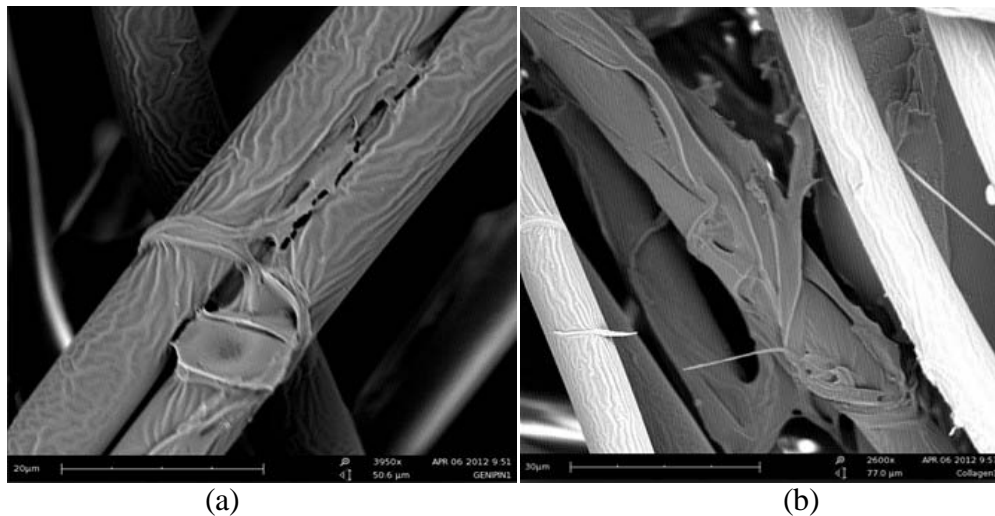


Figure 4.32. SEM image of PLA after genipin attachment (a) and collagen immobilization (b) at 5000X

Figure 4.32 (a) after genipin attachment shows a thicker coating on the PLA fibers compared to the acrylamide treated sample. However, some of these deposits are lumpy when viewed at 5000X magnification. These images suggest that the genipin has been successfully attached to the fibers' surface. Figure 4.32 (b) after collagen immobilization also shows a non-uniform fiber surface with localized deposits. In other places the fibers do not appear to be covered with very much material. So while it can be concluded that collagen has been successfully immobilized on the PLA surface, the deposition does not appear to be very uniform.

The average diameter of the PLA fibers was measured and is presented in Figure 4.33. It shows an increasing trend in fiber diameter after each treatment step. This suggests that the acrylamide, genipin and collagen have all been successfully attached to the surface of PLA fibers without any significant erosion of the PLA fiber surface during these steps. However, the standard deviation for the diameter of the acrylamide activated fibers is larger than for the other three groups. This confirms the previous observation that the deposition of acrylamide on the PLA fiber surface was not so uniform.

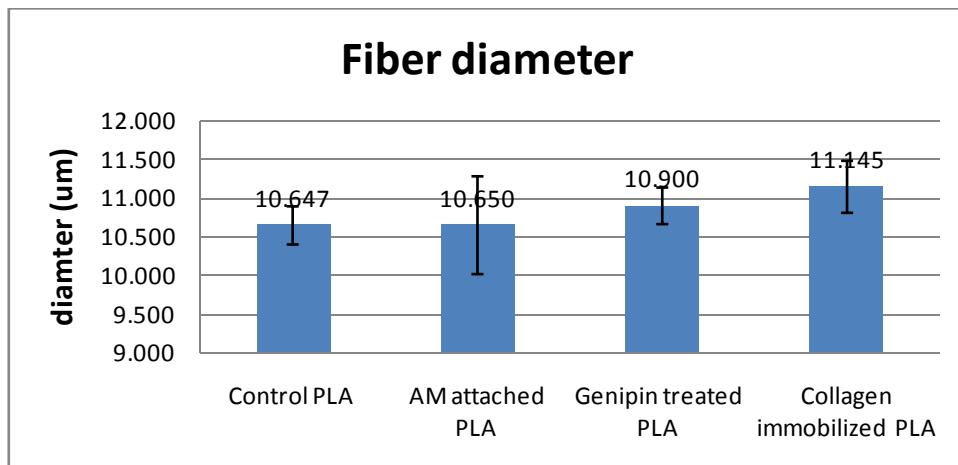


Figure 4.33. Diameter of PLA fibers before and after treatments

4.5. Mechanical Properties

In order to find out how the chemical modifications and treatments changed the mechanical properties and how significant they were, bursting strength tests were carried out on the for different groups of PLA nonwoven fabric.

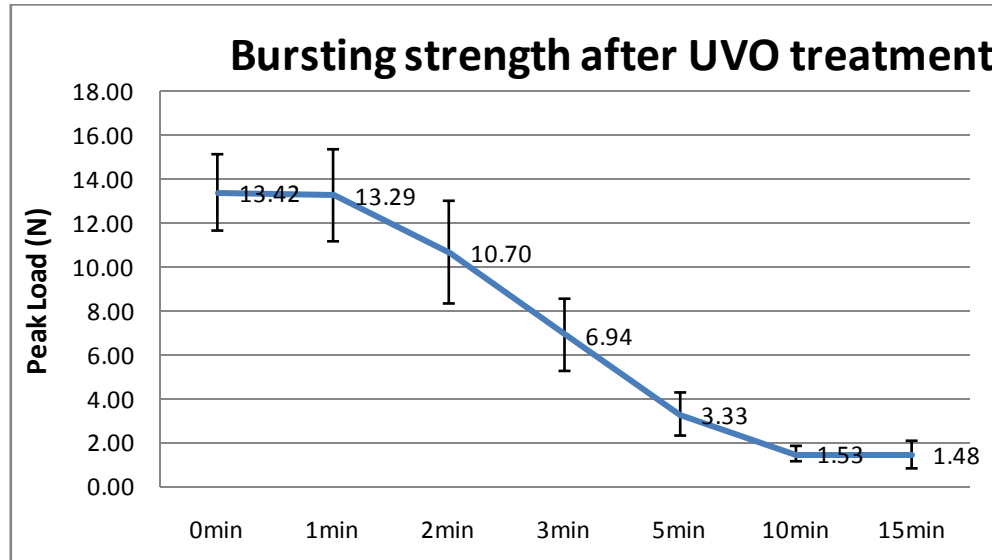


Figure 4.34. Bursting strength of PLA fabric after UVO irradiation

As shown in Figure 4.34, the original PLA control fabric had an average bursting strength of 13.42N. When irradiated by UVO from 1 min to 15 min, the bursting strength decreased to almost zero. The bursting strength dropped by 20% at 2min and by 89% after 10min. The results suggest that exposure to UVO for more than one minute is damaging to PLA fabric and causes the fibers to degrade and break.

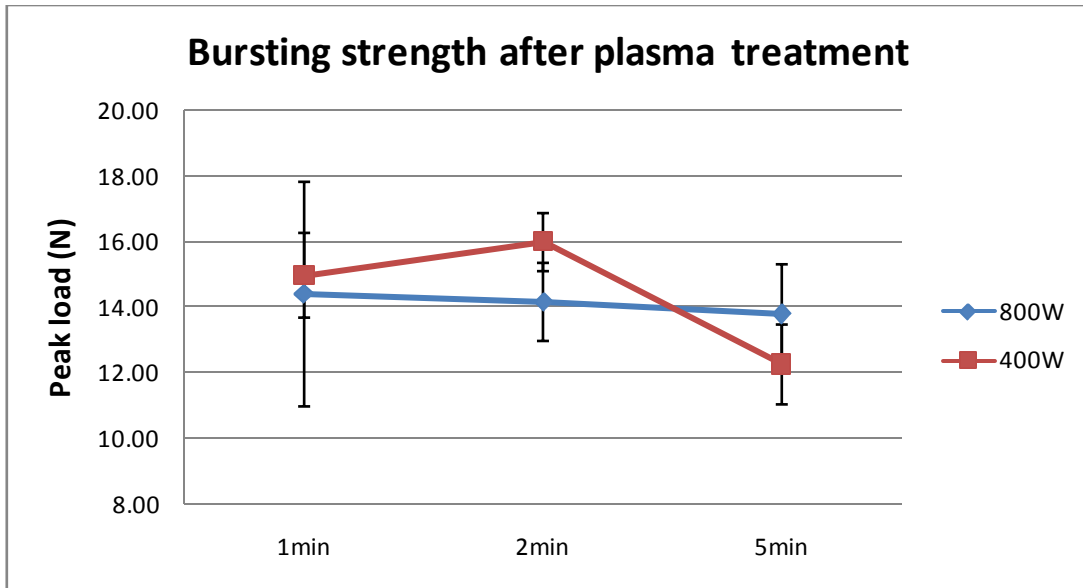


Figure 4.35. Bursting strength of PLA fabric after plasma irradiation

After plasma treatment, the bursting strength of the PLA fabric appeared to have a decreasing trend which is less severe drastic than that of the UVO irradiated samples (Figure 4.35). The bursting strength of the PLA samples exposure to 800W of plasma decreased by 4.3% after 5 min exposure, whereas under 400W of plasma intensity it fell by 18.2%. After UV exposure the bursting strength results showed a similar trend (Figure 4.36). It is therefore concluded that there is no significant change in bursting strength for up to 5 minutes of exposure to plasma or UV irradiation.

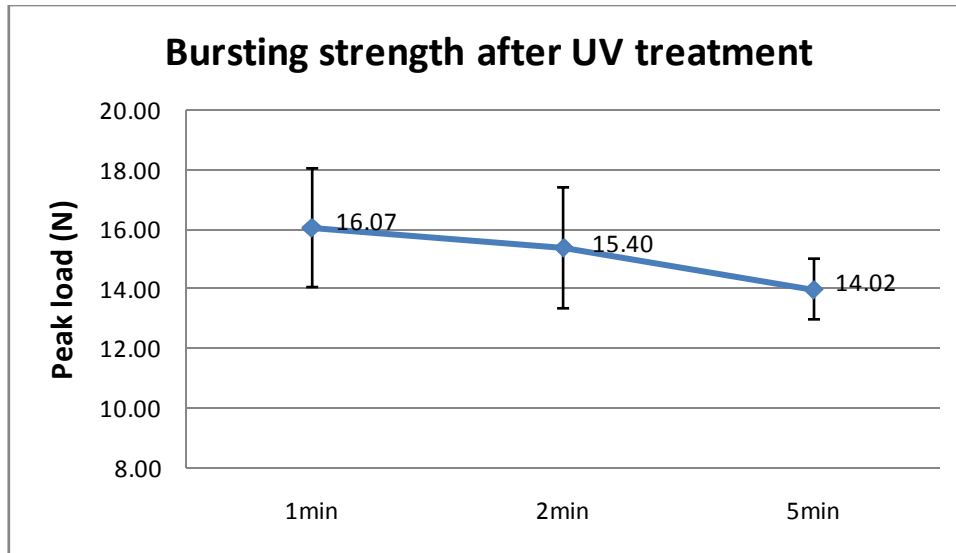


Figure 4.36. Bursting strength of PLA fabric after UV irradiation

In order to make a comparison between the effects of three surface modification treatments on the resulting PLA bursting strength, Figure 4.37 was generated. The samples irradiated by UVO had significant reductions in bursting strength regardless of the duration of irradiation, but this was not the case with plasma and UV treatments. These results and trends indicate that plasma and UV irradiation are less damaging than UVO exposure.

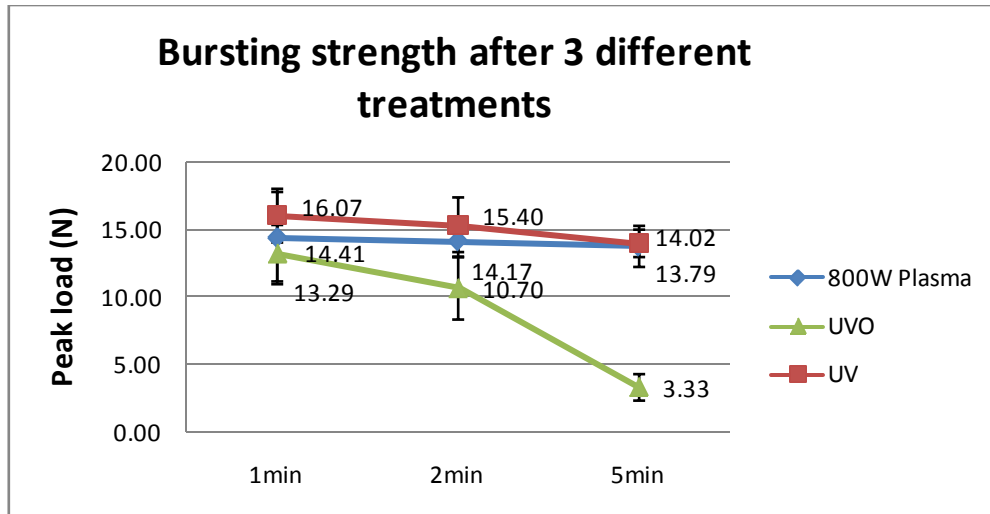


Figure 4.37. Comparison of bursting strength of PLA fabric after three different treatments

To further investigate how genipin attachment and collagen immobilization affected the mechanical properties of the PLA fabric, bursting tests were also carried out after the genipin and collagen treatments of the UVO irradiated and polyacrylamide functionalized PLA fabric. The results are given in Figure 4.38.

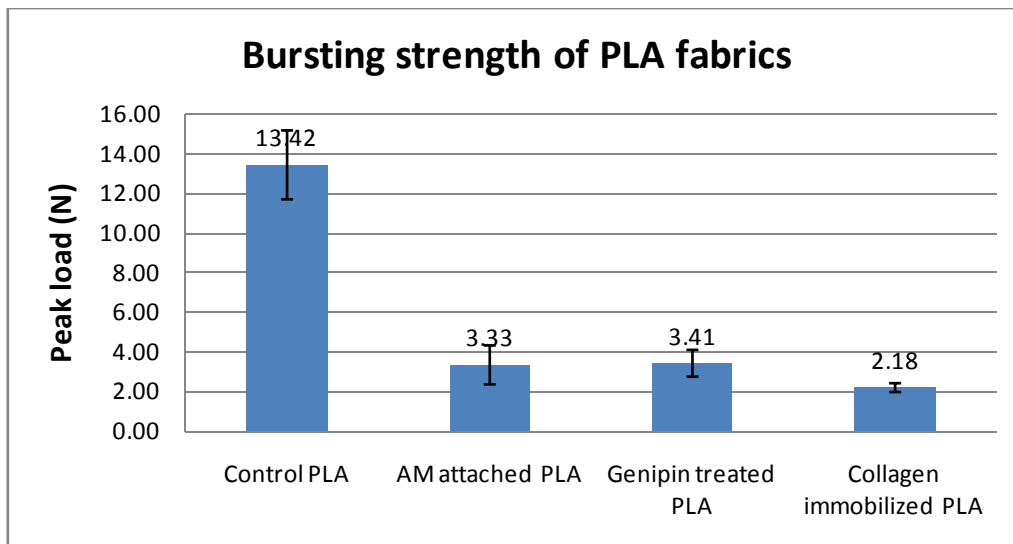


Figure 4.38. Bursting strength of PLA fabric before and after treatments

It can be seen that UVO irradiation causes considerable damage to the PLA fabric since the bursting strength was reduced by 75%. However, the genipin treatment caused a minor increase in the average bursting strength to 3.41N and the collagen immobilization caused a decrease in the bursting strength to 2.18N. One of the reasons for this strength reduction for the collagen immobilized sample is that the acetic acid solvent serves as a catalyst for PLA degradation.

CHAPTER 5-CONCLUSIONS AND RECOMMENDATIONS

5.1. Conclusions

- 1). The three surface modification techniques using UV, UVO and plasma irradiation, all changed the surface properties of the PLA fabric and improved its hydrophilicity to some extent. However, the UVO and 800W plasma irradiation techniques were more effective than the other approaches since the contact angle values decreased by a significant amount and they allowed effective attachment of genipin and collagen to the PLA surface.
- 2). a. For the UVO initiated polymerization, the rate of polymerization increased with monomer concentration as well as with irradiation time. However, longer exposure times to UVO damaged the fibers physical properties. So there needs to be a compromise between the extent of surface modification and the maintenance of mechanical performance. The bursting strength is decreased by more than 50% after 3 minutes of UVO irradiation.
- b. For the plasma initiated polymerization, the rate of polymerization also increased with increasing plasma intensity, monomer concentration as well as exposure time. Meanwhile, plasma created by helium gas alone proved to be more effective in initiating polymerization than a combined helium and oxygen mixture. As a result, the optimal processing conditions were found to be a 5 minute exposure to helium plasma with an 800W power intensity.
- c. The UV initiated polymerization did not provide significant evidence of effective polymerization within a 5 minute period of irradiation exposure.

- 3). The results from the bursting strength tests showed that only the samples irradiated by UVO lost a significant amount of strength, while those exposed to UV and plasma maintained the same strength level. This indicates that UVO can cause damage to PLA fibers and fabric.
- 4). Genipin, the spacer molecule of natural origin, was effectively attached to the functionalized PLA fabric surface as proven by FTIR and TOF-SIMS analysis.
- 5). TOF-SIMS analysis confirmed that collagen was successfully immobilized onto the genipin attached PLA surface. In further studies this collagen layer will improve the biocompatibility and extent of cell proliferation when compared to the original PLA control fabric.

5.2. RECOMMENDATIONS

In the future, the following suggestions may provide fruitful directions for further study:

1. Cell culture tests should be performed to confirm the improved biocompatibility of the collagen immobilized PLA fabric.
2. More variables should be taken into account for UV initiated acrylamide polymerization, such as monomer concentration, photo initiator concentration and longer exposure time, in order to establish the optimal conditions for using a UV initiator.
3. Other monomers and spacer molecules could be selected, such as maleic acid, vinyl acetate and vinyl alcohol so as to determine whether they give better performance

- than acrylamide on PLA nonwoven fabric.
4. Different textiles structures, such as knitted woven, braided and three dimensional fabrics prepared in our laboratory from PLA yarn could serve as alternative substrates for surface modification since they have more diverse mechanical, handling and physical properties than nonwoven fabrics.
 5. Substrates materials other than PLA could be investigated in further study. Some examples of resorbable and biodegradable polymers include PGA, PCL as well as PDO.

REFERENCES

- [1]. Langer R, Vacanti JP. Tissue engineering. *Science*. 1993;260(5110):920-928.
- [2]. R.M.Rasal. "Poly(lactic acid) Modifications". *Progress in Polymer Science*. 2010; 35(3): 338-356.
- [3]. Auras R, Harte B, Selke S. "An overview of polylactides as packaging materials". *Macromol Bioscience*. 2004; 4:835-864.
- [4]. Vacanti JP. Beyond transplantation. Third annual Samuel Jason Mixer lecture. *Archives of Surgery*. 1988;123:545-549.
- [5]. Fuchs Julie R, Nasser Boris A, Vacanti Joseph P, et al. Tissue Engineering: A 21st Century Solution to Surgical Reconstruction. *The Annals of Thoracic Surgery*. 2001; 72(2): 577 – 591.
- [6]. Vacanti CA, and Vacanti JP. Functional organ replacement: the new technology of tissue engineering. *Surgical Technology International*. 1991; 43-49.
- [7]. Vacanti, Charles A. History of Tissue Engineering and A Glimpse Into Its Future. *Tissue Engineering*. 2006; 12(5): 1137 – 1142.
- [8]. Wikipedia. Web. 15 Jan 2012.
<http://en.wikipedia.org/wiki/Tissue_engineering>
- [9]. Ballyns Jeffrey J, Doran Robert F, Archer Shivaun D, Bonassar Lawrence J, et al. An introduction to tissue engineering using hydrogels. *Science Scope*. 2011; 35(1): 50 - 56
- [10]. Wikipedia. Web. 19 Jan 2012. <http://en.wikipedia.org/wiki/Tissue_scaffold#Scaffolds>
- [11]. Wolfe Patricia S, Sell Scott A, Bowlin Gary L, et al. Natural and Synthetic Scaffolds. *Tissue Engineering*. 2011; 41 - 67
- [12]. Freed LE, Vunjak-Novakovic G, Biron RJ, Eagles DB, Lesnoy DC, Barlow SK, et al. Biodegradable polymer scaffolds for tissue engineering. *Nature biotechnology*. 1994; 12:689-693.
- [13]. Web. 19 Jan 2012. <<http://www.bocascientific.com/3dfect-for-3d-scaffolds-p-4757.html>>
- [14]. Tateishi T, Chen G, Ushida T et al. Biodegradable porous scaffolds for tissue engineering. *Journal of Artificial Organs*. 2002; 5(2): 77 – 83.

- [15]. Griffith CK, Miller C, Sainson RC, Calvert JW, Jeon NL, Hughes CC, et al. Diffusion limits of an in vitro thick prevascularized scaffold. *Tissue Engineering*. 2005; 11(1/2):257–266.
- [16]. Ottani V, Raspanti M, Ruggeri A. Collagen structure and functional implications. *Micron*. 2001; 32(3):251–260.
- [17]. Hulmes DJ. Building collagen molecules, fibrils, and suprafibrillar structures. *Journal of Structural Biology*. 2002; 137(1):2–10.
- [18]. Rosso Francesco, Marino Gerardo, Giordano Antonio, Barbarisi Manlio, et al. Smart Materials as Scaffolds for Tissue Engineering. *Journal of Cellular Physiology*. 2005; 203(3): 465 – 470.
- [19]. Boland ED, Espy PG, Bowlin GL. Tissue engineering scaffolds. *Encyclopedia of Biomaterials and Biomedical Engineering*. 2004; 1–9.
- [20]. Mikos AG, Temenoff JS. Formation of highly porous biodegradable scaffolds for tissue engineering. *Electronic Journal of Biotechnology*. 2000; 3(2):114–119.
- [21]. Yang F, et al. Electrospinning of nano/micro scale poly(L-lactic acid) aligned fibers and their potential in neural tissue engineering. *Biomaterials*. 2005; 26(15):2603–2610.
- [22]. Barnes CP, et al. Nanofiber technology: designing the next generation of tissue engineering scaffolds. *Advanced Drug Delivery Reviews*. 2007; 59(14):1413–1433.
- [23]. Zarkoob S, et al. Structure and morphology of electrospun silk nanofibers. *Polymer*. 2004; 45(11):3973–3977.
- [24]. Darling Andrew, Shor Lauren, Khalil Saif, et al. Multi-material scaffolds for Tissue Engineering. *Macromolecular Symposia*. 2005; 227(1): 345 - 356
- [25]. Zisch AH, Lutolf MP, Ehrbar M, Raeber GP, Rizzi SC, Davies N, Schmokel H, Bezuidenhout D, Djonov V, Zilla P, Hubbell JA. Cell-demanded release of VEGF from synthetic, biointeractive cell ingrowth matrices for vascularized tissue growth. *Federation of American Societies for Experimental Biology Journal*. 2003; 17:2260–2262.
- [26]. Halstenberg S, Panitch A, Rizzi S, Hall H, Hubbell JA. Biologically engineered protein-graft-poly(ethylene glycol) hydrogels: A cell plasmindegradable biosynthetic material for tissue repair. *Biomacromolecules*. 2002; 3:710–723.
- [27]. Ikada Y. Surface modification of polymers for medical applications. *Biomaterials*. 1994; 15(10): 725 – 736.

- [28]. Goddard JM, Hotchkiss JH. Polymer surface modification for the attachment of bioactive compounds. *Progress in Polymer Science*. 2007; 32(7): 698 – 725.
- [29]. Decker C, Zahouily K. Light-stabilization of polymeric materials by grafted UV-cured coatings. *Polymer Science: Part A: Polymer Chemistry*. 1998; 36(14): 2571–2580.
- [30] Pan B, Viswanathan K, Hoyle CE, Moore RB. Photoinitiated grafting of maleic anhydride onto polypropylene. *Polymer Science: Part A: Polymer Chemistry*. 2004; 42(8): 1953–1962.
- [31]. Deng Jianping, Wang Lifu, Liu Lianying, Yang Wantai. Developments and new applications of UV-induced surface graft polymerizations. *Progress in Polymer Science*. 2008; 34(2): 156-193.
- [32]. Vig John R, LeBus John W. UV/Ozone Cleaning of Surfaces. *IEEE Transactions on Parts, Hybrids, and Packaging*. 1976; 12(4): 365 – 370.
- [33]. Koo Gwang-Hoe, Jang Jinho. Surface Modification of Poly(Lactic Acid) by UV/Ozone Irradiation. *Fibers and Polymers*. 2008; 9(6): 674 – 678.
- [34]. Kim Eun-Min, Jang Jinho. Surface Modification of Meta-aramid Films by UV/ozone Irradiation. *Fibers and Polymers*. 2010; 11(5): 677 – 682.
- [35]. Grace Jeremy M, Gerenser Louis J. Plasma Treatment of Polymers. *Journal of Dispersion Science and Technology*. 2003; 24(3-4): 305 – 341.
- [36]. Chu PK, Chen JY, Wang LP, Huang N. Plasma-surface modification of biomaterials. *Materials Science & Engineering*. 2002; 36(5): 143 – 206.
- [37]. Schutze A, Jeong JY, Babayan SE, Jaeyoung Park, Selwyn GS, Hicks RF. The Atmospheric-Pressure Plasma Jet: A Review and Comparison to Other Plasma Sources. *IEEE Transactions on Plasma Science*. 1998; 26(6): 1685 – 1694.
- [38]. Oehr Christian. Plasma surface modification of polymers for biomedical use. *Nuclear Instruments and Methods in Physics Research B*. 2003; 208: 40 – 47.
- [39]. Ma Zuwei, Gao Changyou, Ji Jian, Shen Jiacong. Protein immobilization on the surface of poly-L-lactic acid films for improvement of cellular interactions. *European Polymer Journal*. 2002; 38(11): 2279 – 2284.
- [40]. Valuev IL, Chupov VV, Valuev LI. Chemical modification of polymers with physiologically active species using watersoluble carbodiimides. *Biomaterials* 1998; 19: 41–43.

- [41]. Nakajima K, Hirano Y, Iida T, Nakanima A. Adsorption of plasma proteins on Arg-Gly-Asp-Ser peptide-immobilized poly(vinyl alcohol) and ethylene-acrylic acid copolymer films. *Polymer*. 1990; 22: 985–090.
- [42]. Kato Koichi, Kikumura Yoshihito, Yamamoto Masaya, Tomita Naohide, et al. Collagen immobilization onto the surface of artificial hair for improving the tissue adhesion. *Journal of Adhesion Science and Technology*. 2000; 14(5): 635-650.
- [43]. Web. 22 Jan 2012. <http://www.google.com/imgres?hl=zh-CN&gbv=2&tbm=isch&tbid=q_HjrAXbHYtRDM:&imgrefurl=http://www.medical-artist.com/cellular-illustrations.html&docid=UhPMjVvO3KwY_M&imgurl=http://www.medical-artist.com/assets/images/Collagen-Structure.jpg&w=341&h=500&ei=g28kT-3YL4fI0QHOS-SyCA&zoom=1&iact=hc&dur=2&sig=106544341337815064711&page=1&tbnh=132&tbnw=90&start=0&ndsp=21&ved=1t:429,r:5,s:0&tx=97&ty=146&vpx=938&vpy=145&hovh=272&hovw=185&biw=1280&bih=637>
- [44]. Nimni ME, Cheung D, Strates B, Kodama M, Sheikh K. “Bioprosthesis derived from cross-linked and chemically modified collagenous tissues. ” *Collagen, Volume III*. Boca Raton, FL: CRC Press; 1988; 1–38.
- [45]. Cipriano PR, Billingham ME, Oyer PE, Kutsche LM, Stinson EB. Calcification of porcine prosthetic heart valves: A radiographic and light microscopy study. *Circulation*. 1982; 66(5):1100–1104.
- [46]. Schoen FJ, Harasaki H, Kim KM, Anderson HC, Levy RJ. Biomaterial-associated calcification: Pathology, mechanisms, and strategies for prevention. *Journal of Biomedical Materials Research*. 1988; 22(A1):11–36.
- [47]. Sung Hsing-Wen, Chang Wen-Hisang, Ma Chiun-Yuang, Lee Meng-Horng. Crosslinking of biological tissues using genipin and/or carbodiimide. *Journal of Biomedical Materials Research Part A*. 2003; 64(A3): 427 – 438.
- [48]. Griffiths Peter R, De Haseth James A. Fourier transform infrared spectrometry. 2nd Edition. *Chemical Analysis*. 2007; 171, xvii, 529.
- [49]. Griffith PR, de Haseth JA. Fourier transform infrared spectroscopy. Wiley, New York. 1986.
- [50]. Web. 28 Jan 2012. < <http://www.wavesignal.com/Forensics/FTIR.html> >
- [51]. Berthomieu Catherine , Hienerwadel Rainer. Fourier transform infrared (FTIR) spectroscopy. *Photosynthesis Research*. 2009; 101(2-3): 157 – 170.

- [52]. Web. 30 Jan 2012. <http://shop.perkinelmer.com/content/technicalinfo/tch_ftiratr.pdf>
- [53]. Kwok DY, Neumann AW. Contact angle measurement and contact angle interpretation. *Advances in Colloid and Interface Science*. 1999; 81(3): 167 – 249.
- [54]. Eustathopoulos N, Nicholas MG, Drevet B. Wettability at high temperatures. *Pergamon Materials Series*. Oxford, UK. 1999; 3, xv, 420.
- [55]. Knoll, Max. "Aufladepotential und Sekundäremission elektronenbestrahlter Körper". *Zeitschrift für technische Physik*. 1935; 16: 467–475.
- [56]. Web. 31 Jan 2012. < <http://www.purdue.edu/rem/rs/sem.htm> 2.9>
- [57]. Hannes Michler. "Scanning Electron Microscopy (SEM)." *Electron Microscopy of Polymers*. Springer, 2008. 81-120. Web. 10 Feb. 2012.

<<http://www.springerlink.com.prox.lib.ncsu.edu/content/n3wn502154784h84/>>
- [58]. Fadley CS. X-ray photoelectron spectroscopy: Progress and perspectives. *Journal of Electron Spectroscopy and Related Phenomena*. 2010; 178: 2 – 32.
- [59]. Dieter Pleul, Frank Simon. "X-Ray Photoelectron Spectroscopy." *Polymer Surfaces and Interfaces*. SpringerLink, 2008; 71-89. Web. 10 Feb. 2012.
<<http://www.springerlink.com.prox.lib.ncsu.edu/content/q0214308268x742p/>>
- [60]. Web. 3 Feb 2012. < <http://en.wikipedia.org/wiki/File:System2.gif>>
- [61]. A. M. Belu, D. J. Graham, D. G. Castner, "Time-of-Flight Secondary Ion Mass Spectrometry: Techniques and Applications for the Characterization of Biomaterial Surfaces", *Biomaterials*. 2003; 24: 3635 – 3653.
- [62]. Web. 3 Mar 2012. <<http://www.phi.com/surface-analysis-techniques/tof-sims.html>>
- [63]. Song Liu. "Surface Interpenetrating Networks of Poly(ethylene terephthalate) and Polyamides for Effective Biocidal Properties". *Macromolecules Chemistry and Physics*. 2010; (211): 286–296.
- [64]. Tsai CC, Huang RN, Sung HW, Liang HC. "In vitro evaluation of the genotoxicity of a naturally occurring crosslinking agent (genipin) for biologic tissue fixation". *Journal of Biomedical Material Research*. 2000; 52(1):58–65.
- [65]. A. M. Belu, D. J. Graham, D. G. Castner, "Time-of-Flight Secondary Ion Mass Spectrometry: Techniques and Applications for the Characterization of Biomaterial Surfaces", *Biomaterials*, 2003, (24): 3635 – 3653.

APPENDIX

APPENDIX A

Contact angle measurements

1. UVO

a. Sequence Variable

	1	2	3	4	5	Average	Std	CV(%)
Immersion first	65.13	51.81	62.85	51.20	52.16	56.63	6.78	11.96
UVO first	123.12	129.29	127.95	128.08	130.85	127.86	2.89	2.26
Control	126.25	127.80	132.06	129.09	127.89	128.62	2.17	1.69

b. Time variable

1mol/L acrylamide immersion

	1	2	3	4	5	Average	Std	CV(%)
A1-1min	133.40	126.57	123.79	125.34	123.76	126.57	3.99	3.15
A2-2min	127.71	125.04	122.34	123.23	113.97	122.46	5.17	4.22
A3-3min	112.61	114.28	117.33	105.39	120.17	113.96	5.60	4.91
A4-5min	65.13	51.81	62.85	51.20	52.16	56.63	6.78	11.96
B1-10min	29.80	47.56	35.50	39.26	37.28	37.88	6.46	17.05
B2-15min	42.27	30.45	29.48	25.31	38.19	33.14	6.91	20.84

No acrylamide immersion

	1	2	3	4	5	Average	Std	CV(%)
A0-0min	126.25	127.80	132.06	129.09	127.89	128.62	2.17	1.69
A1-1min	122.78	125.36	124.14	128.50	132.20	126.60	3.78	2.99
A2-2min	125.60	134.09	125.30	128.74	123.00	127.35	4.29	3.37
A3-3min	118.35	134.82	124.18	119.62	121.47	123.69	6.60	5.33
A4-5min	118.59	124.66	122.56	114.05	115.83	119.14	4.45	3.74
B1-10min	124.73	125.01	119.28	123.67	116.64	121.87	3.72	3.05
B2-15min	129.61	118.48	125.42	126.72	118.03	123.65	5.16	4.17

c. Monomer concentration variable

	1	2	3	4	5	Average	Std	CV(%)
A4-0mol/L AM	118.59	124.66	122.56	114.05	115.83	119.14	4.45	3.74
C1-0.33mol/L AM	116.57	97.59	97.33	111.56	117.25	108.06	9.92	9.18
C2-0.67mol/L AM	86.37	109.88	103.49	106.4	98.34	100.90	9.16	9.07
A4-1mol/L AM	65.13	51.81	62.85	51.20	52.16	56.63	6.78	11.96

2. Plasma

400W 99.5%He + 0.5%O₂

	1	2	3	4	5	Average	Std	CV(%)
1min	130.31	123.58	126.02	125.79	120.59	125.26	3.57	2.85
2min	118.41	120.26	124.61	121.87	119.3	120.89	2.44	2.02
5min	114.87	118.46	120.45	114.63	110.26	115.73	3.92	3.39

400W He

	1	2	3	4	5	Average	Std	CV(%)
1min	124.07	117.70	125.05	113.83	128.73	121.88	6.00	4.92
2min	114.68	106.03	95.56	104.94	109.32	106.11	7.01	6.60
5min	87.81	101.21	93.52	108.87	103.23	98.93	8.30	8.39

800W He

	1	2	3	4	5	Average	Std	CV(%)
1min	107.93	94.91	94.31	105.65	90.63	98.69	7.62	7.72
2min	63.91	73.65	77.71	107.07	103.11	85.09	18.99	22.31
5min	29.94	20.62	42.79	29.33	41.01	32.74	9.16	27.99

800W He 1 min

	1	2	3	4	5	Average	Std	CV(%)
0.33mol/L AM	130.11	118.33	120.29	129.40	125.81	124.79	5.31	4.25
0.67mol/L AM	114.70	109.35	124.91	119.62	122.93	118.30	6.32	5.35
1mol/L AM	107.93	94.91	94.31	105.65	90.63	98.69	7.62	7.72

800W He 2min

	1	2	3	4	5	Average	Std	CV(%)
0.33mol/L AM	124.18	112.57	124.42	111.23	117.17	117.91	6.23	5.29
0.67mol/L AM	113.78	79.86	121.35	109.29	108.25	106.51	15.76	14.80
1mol/L AM	63.91	73.65	77.71	107.07	103.11	85.09	18.99	22.31

800W He 5min

	1	2	3	4	5	Average	Std	CV(%)
0.33mol/L AM	119.54	118.98	121.58	114.21	115.18	117.90	3.10	2.63
0.67mol/L AM	94.28	112.67	110.12	87.81	80.32	97.04	14.03	14.46
1mol/L AM	29.94	20.62	42.79	29.33	41.01	32.74	9.16	27.99

3. UV

	1	2	3	4	5	Average	Std	CV(%)
1min	129.05	130.31	120.22	129.02	128.53	127.43	4.08	3.20
2min	121.75	110.43	111.18	120.60	124.46	117.68	6.44	5.47
5min	117.94	118.43	114.66	105.90	108.25	113.04	5.69	5.04

APPENDIX B

Fiber diameter measurements

	Control PLA	AM attached PLA	Genipin treated PLA	Collagen immobilized PLA
1	10.651	10.904	10.984	11.609
2	10.576	11.039	11.084	11.653
3	10.658	10.697	11.253	11.584
4	10.971	10.238	11.048	10.952
5	10.930	10.371	11.017	10.873
6	10.231	12.000	10.788	10.939
7	10.275	10.248	10.596	10.826
8	10.839	10.670	10.834	11.141
9	10.626	9.590	10.93	10.975
10	10.717	10.740	10.464	10.895
Average	10.647	10.650	10.900	11.145
Std	0.246	0.631	0.236	0.335
CV(%)	2.309	5.92	2.17	3.01

APPENDIX C

Probe bursting measurements

1. Plasma

a. 800W

	1	2	3	4	5	Average	Std	CV(%)
1min	13.58794	13.68161	11.25995	20.27198	13.24162	14.41	3.42	23.75
2min	13.99431	14.55319	15.46612	12.26221	14.57911	14.17	1.19	8.40
5min	16.22942	12.50285	13.83084	12.49358	13.90705	13.79	1.53	11.06

b. 400W

	1	2	3	4	5	Average	Std	CV(%)
1min	14.39687	13.54578	14.27059	16.33101	16.37352	14.98	1.29	8.62
2min	15.30055	17.02671	16.16059	14.89425	16.58331	15.99	0.88	5.53
5min	12.72227	12.12715	10.82633	14.04887	11.59892	12.26	1.22	9.92

2. UVO

	1	2	3	4	5	Average	Std	CV(%)	Load Lost(%)
0min	11.98568	11.51271	14.04263	15.85355	13.70799	13.42	1.74	12.95	0.00
1min	13.79075	14.27172	15.81861	12.2521	10.30972	13.29	2.10	15.77	0.98
2min	11.77617	7.77522	8.68046	12.10272	13.16864	10.70	2.34	21.84	20.26
3min	9.21465	7.74633	6.01962	6.7888	4.90855	6.94	1.64	23.71	48.32
5min	4.30843	3.29764	2.21824	4.3219	2.50605	3.33	0.98	29.48	75.18
10min	1.6204	1.19152	1.98163	1.69131	1.16149	1.53	0.35	22.85	88.60
15min	1.04991	1.54254	1.57187	0.80939	2.44496	1.48	0.63	42.33	88.94

3. UV

	1	2	3	4	5	Average	Std	CV(%)
1min	15.45	17.23	18.95	14.57	14.17	16.07	1.99	12.39
2min	13.55	14.03	17.86	14.22	17.33	15.40	2.03	13.18
5min	12.99	14.70	14.53	12.86	15.02	14.02	1.02	7.26